Isolation and Characterization of Bacterial Polyhydroxybutyrate Inclusions

by

Nina Kshetry

B.S. Environmental Engineering Science
Massachusetts Institute of Technology, June 2004

Submitted to the Department of Civil and Environmental Engineering in partial fulfillment of the requirements for the degree of

Master of Science in Civil and Environmental Engineering
at the
Massachusetts Institute of Technology

June 2006

Signature of Author: _____
Department of Civil and Environmental Engineering
May 26, 2006

Certified by: _____
Dr. ChoKyun Rha
Professor of Biomaterials Science and Engineering
Thesis Supervisor

Certified by: _____
Dr. Edward F. DeLong
Professor of Civil and Environmental Engineering & Biological Engineering
Thesis Reader

Accepted by: _____
Dr. Andrew J. Whittle
Chairman, Departmental Committee for Graduate Students

Isolation and Characterization of Bacterial Polyhydroxybutyrate Inclusions

by

Nina Kshetry

Submitted to the Department of Civil and Environmental Engineering on May 26, 2006 in Partial Fulfillment of the Requirements for the Degree of Master of Science in Civil and Environmental Engineering

ABSTRACT

Polyhydroxybutyrate (PHB) is a carbon reserve found in some bacteria, and under nutrient limiting conditions accumulates intracellularly in the form of inclusion bodies. These inclusions contain proteins, and the PHB within the inclusions exists in an amorphous state. In this study a procedure to recover native PHB inclusions was developed, and the isolated inclusions were characterized using ^{13}C NMR, western blotting, SDS-PAGE, atomic force microscopy, and fluorescence microscopy. A model for the structure of native PHB inclusions is proposed.

Thesis Supervisor: ChoKyun Rha

Title: Professor of Biomaterials Science and Engineering

ACKNOWLEDGEMENTS

My thesis advisor, Professor ChoKyun Rha, once said "An MIT education is like drinking water from a fire hose." While a student in her lab, I often thought of this phrase and how beautifully it captured the essence of the MIT graduate experience. During my time in the Biomaterials Science and Engineering Laboratory, Professor Rha taught me to think thoroughly and concisely, and to always refer back to first principles when understanding a system. I thank her for this valuable research opportunity, and for her continuous support. What I have learned while part of her lab will guide me through future challenges.

Professor Anthony Sinskey and Professor JoAnne Stubbe provided valuable feedback at biweekly meetings, which built a foundation for my experimental work. Discussion with Professor Sinskey improved my experimental designs. Professor Stubbe gave me an appreciation for the complexity of experimental systems and provided detailed advice and strategies for understanding my specific system.

Many members of the Rha and Sinskey labs served as mentors. Dr. Adam Lawrence introduced me to essential experimental tools needed to conduct research, as well provided valuable feedback and insight. Dr. Pasawadee Pradipasena introduced me to atomic force microscopy, and Dr. Laura Willis provided guidance whenever needed. All members of the Rha and Sinskey labs have created a supportive, productive and fun working environment, and I thank them all for making my time in the lab so pleasant.

I would like to thank the MIT Malaysian Biotechnology Partnership Program (MMBPP) for funding and support, without which none of my work would have been possible.

For giving me inspiration, I thank my MIT colleagues, who demonstrate intense passion and enthusiasm for innovation and creativity. In particular, members of the MicrobeFuel Team, BEInG, and the Energy Club have added great breadth and much excitement to my graduate education.

For keeping me sane, believing in me, and providing a constant flow of love and support, I have to thank my family. Their ability to put things into perspective, has given me much needed strength during the rough times.

Finally, I part with two poems inspired by PHB, and thus bid my thesis research a fond farewell.

precious perspectives
amidst vast amorphousness
crystallize slowly

polymerizing
branching onward through spaces
ad infinitum
without expectations
chains merge with untouched places
and voids decimate

TABLE OF CONTENTS

PAGE

TABLE OF FIGURES

TABLE OF TABLES

TABLE OF EQUATIONS

CHAPTER 1.INTRODUCTION AND BACKGROUND

Polyhydroxybutyrate (PHB) is a naturally occurring biodegradable polyester, which accumulates in some bacterial cells as a carbon storage reserve (1). It belongs to a class of optically active bacterial polyoxesters named polyhydroxyalkanoates (PHAs). PHB inclusion bodies were first identified by Lemoigne in 1926 in the bacterial species *Bacillus megaterium* (24). However, it wasn't until the 1960s and 1970s that a significant research effort was applied toward understanding these polymers, resulting in the discovery of a wide range of PHAs (7).

Over 100 different types of PHAs have been identified to date, exhibiting diversity both in monomer size, polymer length and co-polymer composition (29), (48). The molecular weight varies from 200,000 to 3,000,000 Da, depending on the species type and the growth conditions (51). It is this diversity in structural composition that grants a wide range of properties to this family of polymers, which can vary from thermoplastic to elastomeric (28). In light of decreasing petrochemical reserves, and the hazards of plastic accumulation in the environment, many are looking to PHA plastics as a renewable and biodegradable alternative to petrochemical based plastics. In order to develop this biotechnology on a large scale, a better understanding of the intracellular regulation of such structural variables as molecular weight, side group length, and co-polymer composition is essential.

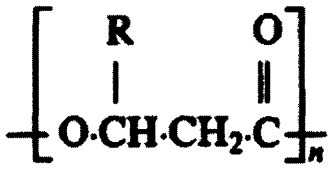

Figure 1. Generic Chemical Formula of Polyhydroxyalkanoates (1).

Figure 2. PHB Biodegradable Objects (25).

PHAs accumulate in the cells within the cytoplasm in the form of inclusion bodies, also referred to as granules (7). By utilizing excess soluble substrate and converting it into insoluble polymeric inclusions, bacteria and other cells are able to maintain low intracellular concentration levels of the soluble monomer, and thus the ability to uptake excess substrate from the extracellular environment through concentration gradients. This mechanism of converting soluble substrate into insoluble polymeric inclusions gives cells the ability to store large quantities of excess substrate intracellularly for use at a later date. Glycogen, starch, polyphosphate, cyanophycin, rubber, and polyhydroxyalkanoates all take the form of inclusion bodies (50).

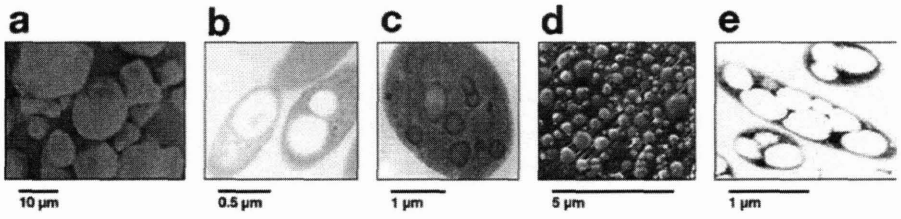

Figure 3. Inclusions (50).

(a) starch in corn (b) polyphosphate in *Vibrio cholerae* (c) cyanophycin in *Aphanocapsa 6308* (d) rubber in *Hevea brasiliensis* (e) PHB in *Cupriavidus necator*.

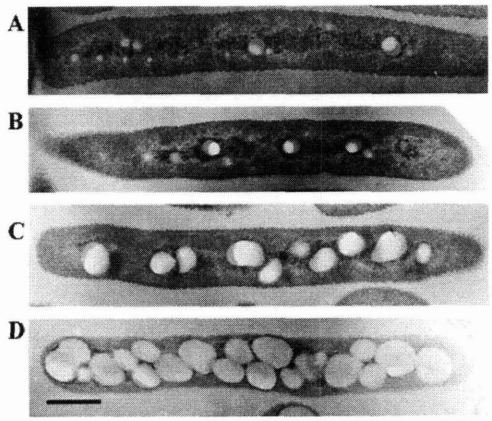

Figure 4. Transmission Electron Microscopy of *C. necator* with PHB Inclusions (55).
Bacteria were cultured with PHB accumulation at (A) 2.5 hr (B) 5 hr (C) 9 hr (D) 24 hr Scale Bar = 5um.

In the case of PHA polymerization, the cell will polymerize excess soluble carbon into PHA inclusions, when some essential nutrient for carbon metabolism, such as nitrogen or oxygen, is lacking in the environment (38). A model organism for PHB biosynthesis is the gram-negative bacteria *Cupriavidus necator* (formerly known as *Ralstonia eutropha*), and it is used in this study. In the presence of excess carbon *C. necator* can accumulate large amounts of PHB up to 90% of the cell dry weight as shown in Figure 4 (51).

PHB is the most studied of all the PHAs, and the mechanisms of PHB polymerization in *C. necator* have been worked out in some detail over the past few decades. Four classes of PHA synthases have been identified to date, and are grouped according to their substrate specificity and subunit composition (39). The Class I synthase, which exists in *C. necator*, is composed of a 65 kDa subunit and acts upon short chain length substrates of hydroxyalkanoates consisting of 3-5 carbon atoms (51). The basic biosynthesis mechanism in *C. necator* involves two other enzymes in addition to the synthase (PhaC); a thiolase (PhaA) and a reductase (PhaB). These three enzymes are encoded in a single operon (35), (36). The biosynthetic pathway for PHB polymerization is outlined in Figure 5 below. The mechanisms involve condensation of acetyl-CoA into acetoacetyl-CoA by PhaA, which is then reduced into hydroxybutyrate-CoA by PhaB, and is finally polymerized into the insoluble PHB via PhaC (25).

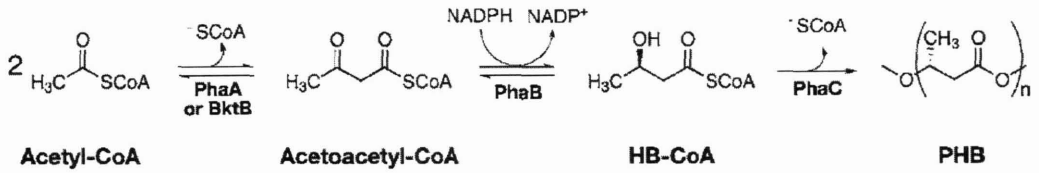

Figure 5. PHB Biosynthetic Pathway (50).

The resulting PHB homopolymer has a molecular weight of around 1,000,000 Da, and a low polydisperisty (53). The PhaC is reused many times during the synthesis of the PHB chains, implying that some regulated termination must occur in order to synthesize this low polydispersity high molecular weight polymer.

PHB depolymerases can be classified as either intracellular or extracellular (16). The intracellular depolymerases cannot act upon crystalline PHB; however, the extracellular depolymerases can act upon both amorphous and crystalline PHB, which is why crystalline PHB based commodity materials are able to degrade in the environment (33).

The highly regular isotactic nature of PHB (Figure 6 and 7 below) is conducive to a high degree of crystallization of between 60 – 80%, which is the highest of all naturally occurring PHAs. Larger monomer units and co-polymers of PHA show significantly less crystallinity than PHB, presumably due to steric hindrances that prevent close packing conformations (1), (56). Despite the fact that pure PHB is likely to exist in a highly crystalline state, PHB in inclusion form is in an amorphous state. This amorphous state of native PHB granules has been shown using two independent techniques, X-ray diffraction and ^{13}C solution state NMR, as both of these techniques can distinguish solid from liquid material (14),(20),(46).

X-ray diffraction is used to study the structure of crystalline material. Lattice spacing in crystals scatter x-rays producing distinct diffraction patterns, which can be analyzed for structural information. Liquids or amorphous materials do not produce diffraction patterns, and therefore can be distinguished from crystalline material (56),(60). ^{13}C NMR is another technique that can differentiate between solid and liquid. It takes much longer to collect spectra from solids than it does from liquids. This result is due to the ability of liquids to reach an excited energy state, and return to equilibrium much faster than solids can. Therefore, under normal acquisition conditions (where collection time is on the order of a few seconds), liquids will display sharp spectra, whereas solids will display broad spectra or no spectra at all (23), (41).

Isolation of PHB by many methods can cause irreversible crystallization of the PHB, and in this denatured state it is no longer accessible to intracellular depolymerases for degradation (51).

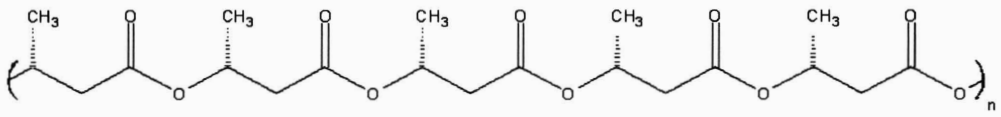

Figure 6. Isotactic Structure of PHB Homopolymer.

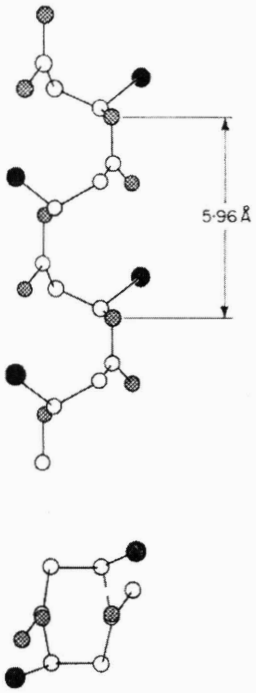

Figure 7. Alpha Helix 3D Structure of PHB Homopolymer (34).

Black = Methyl (CH_3), Grey = Oxygen, White = Carbon. The crystalline form of PHB displays a left handed helix formation with a two-fold screw axis, the repeat unit 0.596nm.

Experiments performed by Horowitz and Sanders indicate the amorphous nature of native PHB is likely due to a surfactant-like coating on the surface of the inclusions, which maintains inclusions as distinct colloidal structures and reduces the likelihood of crystallization(14). It has been demonstrated that certain proteins coat the surface of the granule; in addition a phospholipid layer has been proposed to coat the surface of the granule (3),(4). Key proteins involved in the biosynthesis of PHB have been located at the surface of the inclusions through

immunochemical labeling and enzymatic assays conducted on purified PHB granules (8), (40). These proteins are PhaC, PhaP (or phasin), PHA depolymerases, and PhaR (the negative regulator of PhaP) (38).

PhaP is a noncatalytic protein that is associated with the granule surface, and its expression is correlated with granule size (Figure 9) (11),(44),(58). Recently, three additional phasins have been discovered in *C. necator* based on sequence homology(37). The concentration of PhaP is highly correlated with the production of PHB, and the transcription of *phaP* is induced at the start of nitrogen limited and excess carbon conditions (44). It is thought that PhaP is the major constituent of a stabilization layer surrounding granules, which prevents coalescence of granules within the cell (19),(38),(59). PhaP represents 5% of total protein within the cell when it is grown under conditions of high PHB storage, and covers between 27 – 54 % of the granule surface(53),(58). By contrast, PhaC is believed to cover between 0.5 – 1.2% of the granule surface (53).

Figure 8. Immunochemical labeled PhaC on PHB Inclusions Surface in *C. necator* (8).

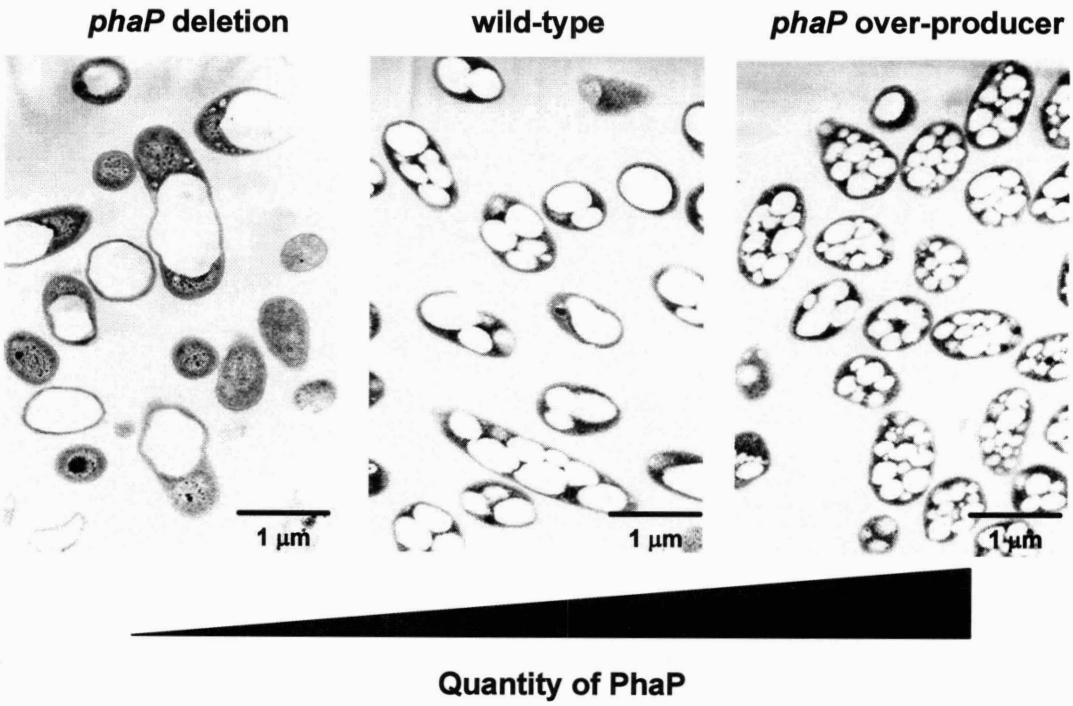

Figure 9. Granule Size as Affected by the Quantity of PhaP (61).

In order to better understand the structure-function relationship of native granules in PHB biosynthesis, an isolation procedure that preserves native state of the PHB inclusions is essential. In this study an isolation technique was developed and characterized with bioanalytical and microscopy tools, and a model for native PHB inclusion morphology is proposed.

CHAPTER 2.MATERIALS AND METHODS

2.1. ISOLATION OF PHB INCLUSIONS FROM *C. NECATOR*

2.1.1. Fermentation for High PHB Production in *C. necator* (PHB_H culture conditions)

The enriched media used for culturing *C. necator* was composed of dextrose free Tryptic Soy Broth (Becton Dickenson, NJ, USA Cat#: 286220) at a concentration of 27.5g/L containing 10μg/ml of gentamicin sulfate (Sigma, St. Louis, MO, Cat# G-3632); referred to as TSB/gentamicin. All strains of *C. necator* employed in this study contained a gentamicin resistance gene. Frozen stocks of *C. necator* were stored at – 80°C. The frozen stocks inoculated onto TSB/gentamicin 2% agar plates were incubated for 48 h at 30°C. One resulting colony was inoculated into a test tube containing 5ml of TSB/gentamicin and incubated for 24 to 48 h at 30°C. From this test tube 2ml of culture was inoculated into a 100ml TSB/gentamicin in a baffled flask and incubated for 24 h at 30°C. This culture was inoculated into 200ml of PHB_H chemically defined media to an initial OD_{600nm} value of 0.5 and was incubated for 24 h at 30°C in a baffled flask. The PHB_H chemically defined media used in this study has been optimized for conditions that allow *C. necator* to produce high amounts of PHB (see formulation below).

2.1.2. PHB_H Chemically Defined Media

A PHB salts solution was prepared by adding to 960ml of deionized water the following: 6.7ml 1.0M sodium phosphate monobasic, 12.9ml 0.5M sodium phosphate dibasic, 5.2ml 0.5M potassium sulfate, and 1ml 1N sodium hydroxide. To 200ml of PHB salts solution the following was added: 2ml 100X magnesium sulfate (3.9g/100ml), 2ml 100X calcium chloride (0.62g/100ml), 200μl of 1000X trace salts stock solution (40mg cupric sulfate 5 H_2O, 240 mg zinc sulfate 7 H_2O, 249mg manganese sulfate 1 H_2O, 1500 mg ferrous sulfate 7 H_2O in a final volume of 100ml 0.1N hydrochloric acid), 4ml of 50% fructose, 200μl of 10% ammonium

chloride, and 200µl of gentamicin (10mg/ml). All solutions, except the gentamicin stock solution, were sterilized by autoclaving before preparing the PHB_H media.

2.1.3. HPLC Quantification for PHB in *C. necator*

New glass tubes (VWR, Westchester, PA, Cat# 47729-576) were dried at 80°C overnight and then weighed. 3 to 15ml samples were placed into the glass tubes and centrifuged (Sorvall, Asheville, NC, RC 5C PLUS centrifuge, SS-34 rotor and rubber adaptors) at 5000rpm for 5 min at 4°C. The resulting pellet was washed with the original volume of ice-cold H_2O. The centrifugation step was repeated, the supernatant was pipetted off, and the glass tube was placed in a vacuum oven at 80°C to dry overnight. The weight of the dried pellet and glass tube was recorded. 30mg of PHB was measured into a glass tube for use as a standard (Aldrich, St. Louis, MO, Cat # 363502-100G). 1ml of concentrated H_2SO_4 was added to all samples, which were then boiled for 30 min in a water bath ($T \geq 90°C$). The acid catalyzes depolymerization of PHB with elimination of water to yield crotonic acid, which is then detected using the HPLC. The samples were cooled on ice. The standard was diluted using concentrated H_2SO_4 yielding the following final concentrations of PHB: 10, 3, 1, 0.1, 0.3 mg/ml. 4ml of 0.01N H_2SO_4 (533µl concentrated H_2SO_4/2L H_2O) was added to each sample tube, which was then vortexed gently. 2ml of each sample was filtered into new glass tube using a 5ml syringe with a 0.2µm filter (Gelman, Ann Arbor, MI, Acrodisc LC 13 PVDF 0.2um). 100µl of the filtered samples were transferred to HPLC vials (Agilent, Palo Alto, CA, Cat# 5182-0714) containing 900µl of 0.01N H_2SO_4. The HPLC was run with a 25µl injection volume at 50°C for 40 min on a Biorad Aminex HPX-87H organic acid column and crotonic acid was detected at 210nm (Biorad, Hercules, CA).

2.1.4. Native PHB Inclusions Isolation with Sonication Followed by Filtration

C. necator was grown for 24 h using standard conditions for high PHB accumulation as outlined above. 10ml of the culture was removed and centrifuged (5500rpm, 5 min, 4°C). The

supernatant was discarded and the pellet was resuspended in 10ml of 0.85% saline. The suspension was recentrifuged, and the pellet was finally suspended in 5ml of Tris buffer (pH 7.5) and taken for sonication (Misonix, Inc, Farmingdale, NY--formerly Heat Systems, Sonicator Ultrasonic Processor XL). Sonication was performed on ice at 4°C with 3 min of total pulse time (power = 4.5, 30 sec pulse, 15 sec pause). A 0.22μm cellulose acetate filter was used to separate the inclusions from the smaller components of the cellular material (Corning Inc, Corning, NY, Cat# 430626). The cell lysate was filtered through vacuum, and then the filter was washed with minimal amount of PBS (pH 7.3-7.5) in order to retrieve the inclusions from the surface.

2.1.5. Enzymatic Lysis

2.1.5.1. With Salt

50ml of 24 h PHB_H culture was centrifuged (5500 rpm, 5 min, 4°C) and resuspended in 50mgs lysozyme/2ml PBS and incubated at 37°C for 1 h. 0.5 ml of 5M NaCl was added along with 20μl of DNase (Roche Diagnostics, Alameda, CA, Cat# 10 776 785 001) and incubated for 37°C for 1 h. The resulting cell lysate was brought up to a final concentration of 10ml using PBS (EMD Chemicals, Gibbstown, NJ, USA Cat# 6505).

2.1.5.2. Without Salt

24h PHB_H culture was centrifuged (5,500 rpm, 4°C, 5 min) and resuspended in 15-20ml lysis buffer (50mM Tris HCl pH 8, 25mM NaCl, 2mM EDTA) for a final OD_{600} reading of 20-40. The solution was placed at –80°C for approximately 1 h and then thawed at room temperature, after which it was vortexed thoroughly. 1mg/ml final concentration of lysozyme (10mg/ml freshly prepared stock) was added to the solution and it was incubated for 1 h at 37°C. 50μl of 4mg/ml DNase, 50μl of 1M $MgSO_4$, and 1ml of protease inhibitor cocktail (Sigma, St. Louis, MO, Cat# P 8465) was added to the solution and it was incubated at 37°C for 1 h.

2.1.5. PHB Inclusion Isolation by Ultracentrifugation

To a sucrose density gradient (8ml 2.0M, 9ml 1.7M, 8ml 1.5M, and 9ml 1.25M) 3ml of cell lysate was added. 6 tubes were centrifuged at 28,000rpm, 4°C, and 2 h. The 1.5M/1.7M interface bands were collected by piercing the tube with a syringe at the location of the band. The bands of 3 tubes were pooled together and placed in 18-14 cm long dialysis tubing (Spectra/Por, Rancho Dominguez, CA, Cat#:132700) and the inclusions were dialyzed against 2L of dialysis buffer at 4°C for at least 2 h (50mM sodium phosphate pH 8.0, 1mM EDTA). A Beckman L-80 Ultracentrifuge was used with a SW 28 Rotor and Polyallomer tubes of size 25 X 89mm (Beckman, Fullerton, CA).

2.2. CHARACTERIZATION OF PHB INCLUSIONS

2.2.1. PhaP Standard

2.2.1.1. Transformation of Bacteria

1µl of DNA (pGY101) was placed in a test tube and put on ice for a few minutes (63). 20µl of competent BL21 (DE3) *E. coli* cells (Stratagene, La Jolla, CA, Cat# 200131) were placed into the DNA tube and mixed by flicking the tube. The tube was then placed on ice for 5 min. This cell suspension was then placed in a 42°C water bath for 30 sec, and then placed back on ice for 2 min. 80µl of high nutrient broth that had been preheated to 37°C was added to the cell suspension. The cell suspension was placed in a 37°C shaker for 30 min to 1 h. Finally, the solution was used to plate out colonies, using a 2% agar/LB plate with ampillicin (100µg/ml). 50µl of the bacterial solution was used per agar plate. The plates were incubated at 37°C overnight.

2.2.1.2. Induction of Bacteria

A single colony from the LB/ampicillin agar plate was taken and placed into a 50ml LB broth (250ml baffled flask) w/ 50µl ampicillin (100µg/ml) and incubated for 24 h. 8ml from a 50ml sample was placed into a 2.8L baffled flask, with 1L of LB and 1ml of ampicillin. The culture was grown to an OD_{600} of 0.6 to 0.8 (about 2-4 hours). Isopropyl-β-D-thiogalactopyranoside (IPTG) was added to a final concentration of 0.1mM. The culture was spun down (apprx 3.4 g wet weight) and processed directly or placed in -80°C freezer. Better results were obtained if cells were processed fresh instead of frozen.

2.2.1.3. Lysis and Protein Precipitation

Cell pellets were resuspended in 27ml of TE buffer (50mM Tris, 1mM EDTA, pH 7.5) with 1ml of protease inhibitor (Sigma, St. Louis, MO, Cat# P8465). The bacterial solution was run through a French Press at 14,000 psi twice (before second run another 1ml of protease inhibitor was added to solution) (SIM Aminco, Spectronic Systems). The solution was then centrifuged at 25,000 X g for 30 min. To this supernatant ammonium sulfate was gradually added to a final concentration of 3.9g/20ml as the solution was gently mixed at 4°C (35% saturation). The solution was centrifuged at 20,000 X g for 20 min, and the pellet was collected. 500µl of protease inhibitor cocktail was added to the solution, and 0.36g/ml of ammonium sulfate was added gradually, while gently stirring at 4°C (60% saturation). The solution was centrifuged at 25,000 X g for 30 min. The pellet was obtained and resuspended in a minimal amount of TE buffer.

2.2.1.4. Desalting

In order to desalt the solution a Sephadex G-25 column was used with dimensions as follows: column L = 20cm, W = 1.5cm. After ammonium precipitation a total protein content of around 180mg was obtained; and after conducting desalting the total protein content was around 120 mg in 17ml of TE buffer. Six milliliters of this desalted solution was used in the DEAE support column for total of around 40mg protein loaded onto the column.

2.2.1.5. DEAE Support Column

Around 100ml of DEAE support material (Bio-Rad, Hercules, CA, Cat# 156-0020) was poured into beaker and equilibrated with TE buffer. Finally, around 80ml of the DEAE support/TE slurry was packed in a column (L = 15cm, W = 5cm). The protein was added above the solid interface. 40 X 5ml fractions were collected. Fractions 1-24 were collections of the flow through. After the 24th fraction was collected a salt gradient was set up (Figure 10), with TE buffer and 250mM NaCl and fractions 25-40 were collected. SDS PAGE and Spectrophotometric Analysis of fractions were conducted using standard protocols (Agilent, Palo Alto, CA, UV-Vis Spectrophotometer G1115AA).

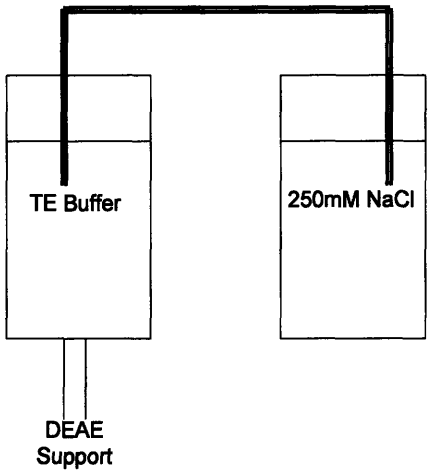

Figure 10. Salt Gradient Set Up.

2.2.2. ^{13}C NMR for Detection of Amorphous PHB

2.2.2.1. Whole Cells

A 24 h culture of *C. necator* in PHB_H chemically defined media (following standard culturing protocol outlined above) was centrifuged at 5500rpm for 5 minutes at 4°C. The supernatant was discarded and the pellet (500 mg of wet weight) was resuspended in 600ul H_2O and 100ul D_2O. This suspension was placed in Wilmad Pyrex NMR tubes (Buena, NJ). The ^{13}C NMR was conducted on an INOVA 501 (Varian, Palo Alto, CA) using the following conditions:

1. T = 60°C

2. Acquisition Time (at) = 4.721 sec
3. Delay Time (d1) = 0.279 sec
4. Recycle Time (at + d1) = 5 sec

The full carbon spectrum was visible after 200 transients of data collection.

2.2.2.2. Purified Inclusions

Purified PHB inclusions (2.1.5.1., 2.1.5.2) were analyzed with ^{13}C NMR. After dialysis the solution was centrifuged at 5500rpm, for 10 min at 4°C. The isolated inclusion pellet was resuspended in 600µl H_2O and 100ul D_2O, which was placed in Wilmad Pyrex NMR tubes (Buena, NJ). The ^{13}C NMR was conducted on an INOVA 501 using the following conditions:

1. T = 60°C
2. Acquisition Time (at) = 4.721 sec
3. Delay Time (d1) = 0.279 sec
4. Recycle Time (at + d1) = 5 sec

The total time transients needed to view full carbon spectrum varies, depending on the concentration of PHB present. Data acquisition can last as little as 2 h to as long as overnight.

2.2.3. Western Blotting

The linear range of detection of PhaP is between 2 and 12ng and the linear range of detection of PhaC is between 0.5 and 4ng. The protein levels of each sample were estimated based on Bradford assay, and diluted/concentrated in order to be detectable within the linear range of detection. The samples were boiled in loading buffer for 30 min. Samples containing PHB were then centrifuged at 13,000 X g for 6 min and the supernatant was used for further analysis. Samples were loaded onto a 15% SDS PAGE gel and run for 70 minutes at 140V in tank buffer (15.1g Tris base, 72.0g glycine, 5.0g SDS, in 1L dH_2O).

The gel was removed and washed in transfer buffer (6.06g Tris base, 28.8g glycine, 1600ml dH_2O) for 30 min. A PVDF membrane (Millpore, Bedford, MA, Cat# IPVH20200) was washed for 15 sec in methanol, 2 min in deionized water, and at least 5 min in transfer buffer before use. The gel/membrane transfer assembly was packed on ice as per manufacturer's

instructions, and the transfer was run for 100 min at 80V. After transfer, the gel was carefully removed and placed in 1X PBS for a few seconds, and then transferred to a tray with blocking buffer (10% casein, 0.1% Tween 20, TAE buffer) and left to rock for 1 h. The membrane was washed with primary antibody (anti-PhaP blood serum: 20,000X stock, anti-PhaC blood serum: 1,000X stock, diluted in blocking buffer) for 1 h (both anti-PhaP and anti-PhaC were rabbit polyclonal). This was followed by 2 X 5 min blocking buffer washes. The membrane was then washed with secondary antibody (all developing reagents were from the Western Light Kit, Applied Biosystems, Bedford, MA, Cat# WL10RC). This was followed by 3 X 5 min blocking buffer washes, and 2 X 2 min assay buffer washes, and finally the membrane was incubated in CSPD substrate solution (3ml/membrane) for 5 min. The membrane was placed in a plastic folder and developed using chemiluminescene high sensitivity (UVP Bioimaging Systems, BioChemi System, Upland, CA).

2.2.3. Zeta Potential

C. necator was grown under PHB_H production conditions. Isolated Inclusions (2.1.5.1., 2.1.5.2) were diluted 10X - 20X with deionized water (I = 0.005), until sample was mostly clear (approximately 0.1- 0.2% w/v). The sample was analyzed using BIC PALS Zeta Potential Analyzer (Brookhaven Instruments Corporation, Holtsville, NY).

2.2.4. Elemental Analysis

C. necator was grown under PHB_H production conditions. Isolated Inclusions (2.1.5.1.) were centrifuged at 5500 rpm for 10 min, resuspended in 4ml of deionized H_2O, and recentrifuged. Supernatant was discarded and a small amount of ethanol was added to the pellet. The pellet was then placed under nitrogen to dry, and the dried sample was sent to Atlantic Microlabs (Norcross, GA) for elemental analysis.

2.3. IMAGING OF PHB INCLUSIONS

2.3.1. Imaging Purified PHB Inclusions

2.3.1.1. Atomic Force Microscopy (TM Explorer)

C. necator was grown using standard PHB_H production conditions and the inclusions were isolated (2.1.4, 2.1.5.2). Isolated inclusions were concentrated 10X - 20X by centrifugation (10,000 rpm, 10 min) and resuspended in deionized water (inclusions isolated with sonication followed by filtration (2.1.4) were used unprocessed and without total protein determination). The total protein content in the concentrated inclusion sample was measured as 0.2-0.6 mg/ml with the Bradford Assay (Bio-Rad, Hercules, CA, Cat# 500-0006). The concentrated inclusions were vortexed and then 25 -50µl were placed on an amino-silane coated slide (Invitrogen, Carlsbad, CA, Cat# 20-1001-25) and incubated for 1 h at room temperature. The slide was washed with deionized water and dried for around 1 h. The slide was then placed under the AFM for contact mode imaging in air (TM Explorer, Veeco, Santa Barbara, CA), using standard SiN_3 contact mode tips (Veeco, Santa Barbara, CA, Cat# MSCT-EXMT-BF).

2.3.1.2. Atomic Force Microscopy (Veeco Multi Mode)

C. necator was grown using standard PHB_H production conditions and the granules were isolated (2.1.5.2.). Isolated inclusions were concentrated 10X - 20X by centrifugation (10,000 rpm, 10 min) and resuspended in deionized water. The total protein content in the concentrated inclusion sample was 0.2 - 0.6 mg/ml as measured with the standard Bradford Assay. Amino silane coated glass slides were cut to approximately 1 X 1cm, and cleansed with nitrogen gas. 25 – 50µl of isolated inclusions were placed on amino silane coated glass slides and incubated for 1 h at room temperature. After incubation the slides was washed with deionized water and dried. The slides were adhered to metal pucks using double sided tape (Ted Pella, Redding, CA, Cat#: 16218). Sample was scanned using Olympus AC240TS silicon probes with Al backside coating (Asylum Research, Santa Barbara, CA). The probes had a resonance frequency of 70 – 80 KHz in air. The scanning was done at a rate of 1 Hz, a setpoint of value of around 1, a proportional gain of 0.5 – 0.8, and an integral gain of 0.3 – 0.6.

2.3.1.3. Fluorescent Microscopy

C. necator was grown using standard PHB_H production conditions and the inclusions were isolated (2.1.5.1, 2.1.5.2). The isolated inclusions were then concentrated 10 - 20X by centrifugation (10,000 rpm, 10 min) and resuspended in deionized water. Inclusions were stained with a mixture of DiO and Nile red (50μg/ml each) and the solution was vortexed vigorously to allow for adequate mixing. DiO and Nile red are both lipophilic dyes; however, DiO cannot penetrate cell membranes whereas Nile red can. 50μl of the stained inclusions were placed on amino silane coated glass slides and allowed to incubate at room temperature for 1 h. The solution was then washed and then a drop of mounting medium (VectaSheild, Burlingame, CA, Cat# H-1200) was placed on the glass slide sealing a cover slip over the slide. The slide was observed with a deconvolution microscope (Olympus IX71, Middlesex, UK).

CHAPTER 3.RESULTS AND DISCUSSION

3.1. ISOLATION OF PHB INCLUSIONS

Standard PHB_H culture conditions for *C. necator* were used to grow the bacteria for a period of 24 h, after which time the culture was analyzed for PHB production using HPLC. The PHB present in *C. necator* expressed as a percentage of cell dry weight is shown in Figure 11. The PHB_H culture conditions were in fact allowing *C. necator* to accumulate significant amounts of PHB in each experiment.

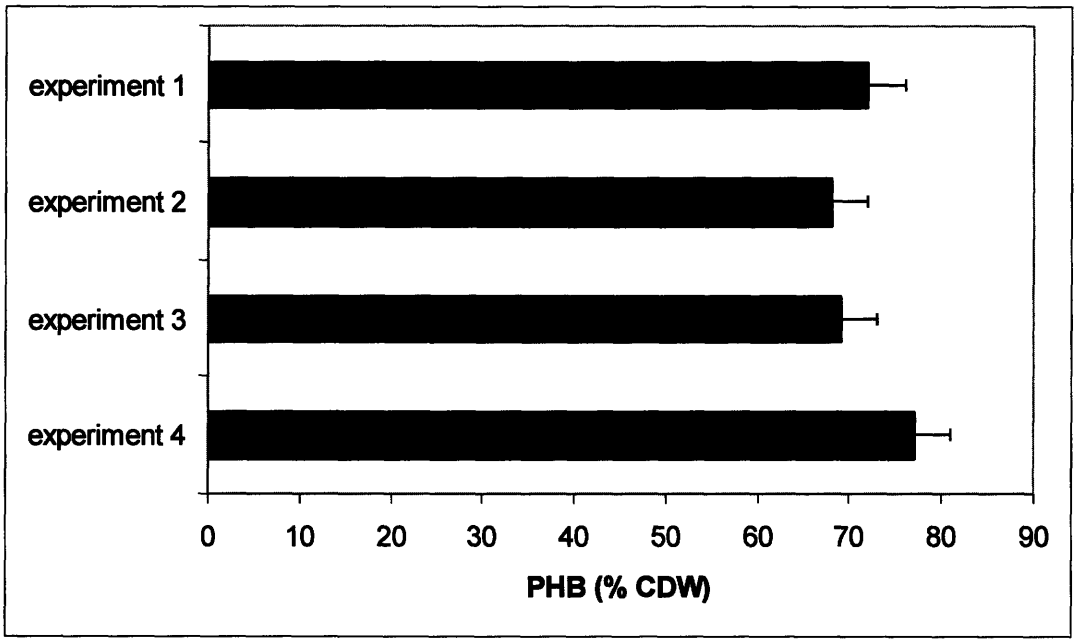

Figure 11. PHB (% of Cell Dry Weight CDW) in *C. necator* after 24 hours under PHB_H growth conditions.

The effectiveness of various lysis techniques was analyzed via fluorescence microscopy and atomic force microscopy (AFM). One of the most common methods of lysis used in the purification of PHB inclusions is sonication. However, we observed that sonication was causing

inclusion aggregation that increased with increasing sonication times, presumably due to the heat generated during the sonication, despite the fact that sonication was conducted on ice. AFM images of granules isolated by sonication and filtration showed that inclusions were aggregating. Furthermore, the sonication did not completely lyse many cells. The AFM images of the inclusions purified via sonication followed by filtration is shown in Figure 12.

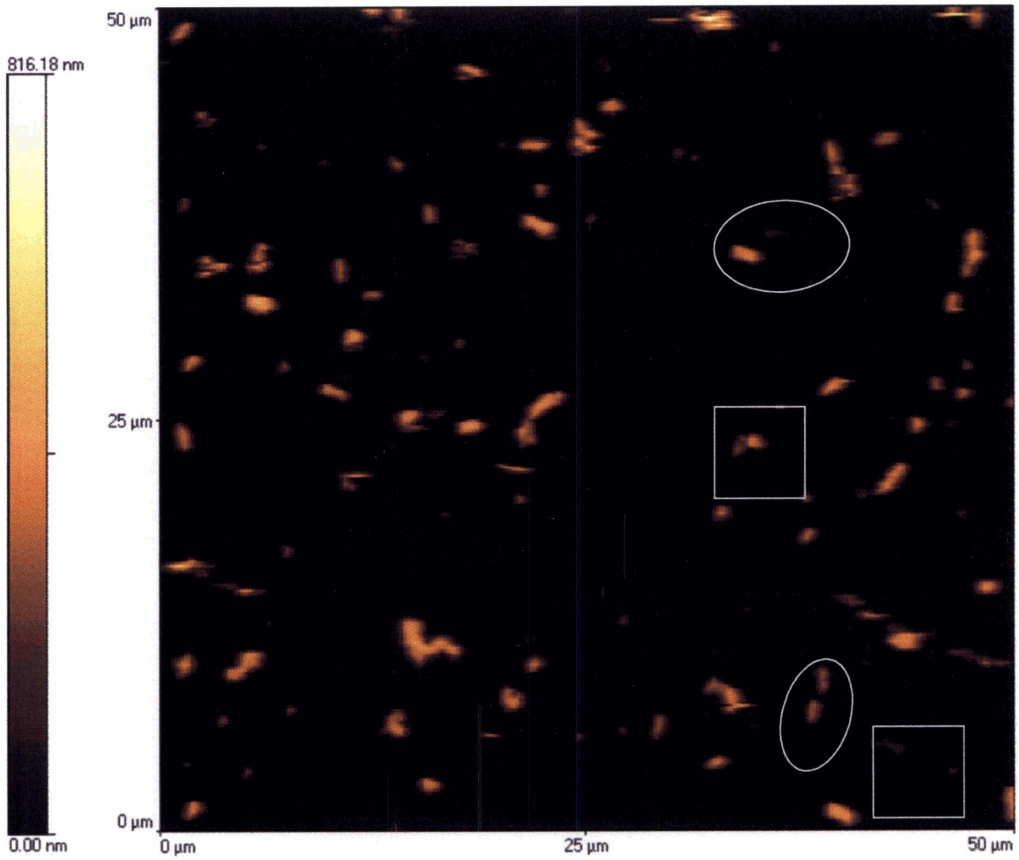

Figure 12. AFM Topography Image of PHB Inclusions Purified Via Sonication Followed by Filtration.

Imaging was conducted in air using contact mode with a scan area of 50 X 50µm. The dark areas represent low points and the light areas represent high points. Clusters of aggregates could be observed as indicated by the boxes. Objects displaying the rod-like morphology of *C. necator* cells could be observed as indicated by the circles. Magnified images of the boxed and circled objects are shown in Figure 13 and 14.

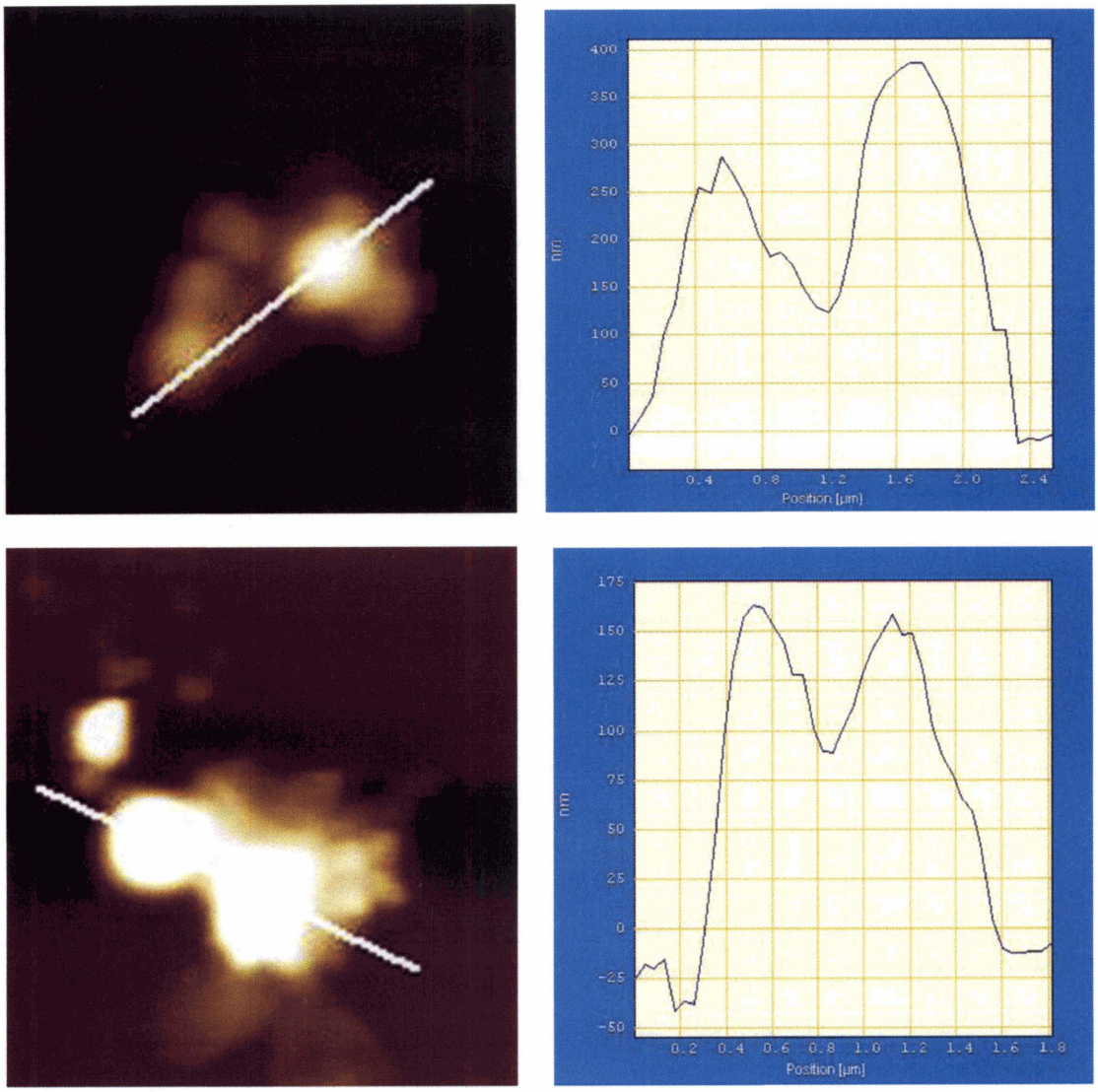

Figure 13. Aggregated PHB Inclusions Topography and Line Profile.

Magnified topography images of aggregated PHB inclusions boxed in Figure 12 (right) and corresponding line profiles (left). The line profiles display the height of the objects along the line drawn on the right. Using the line profile data, the width of the objects is measured to be approximately 500nm, which corresponds to the expected width of PHB inclusions (1). Both the topography and line profile images demonstrate that the space between inclusions remains relatively high, which indicative of PHB aggregation.

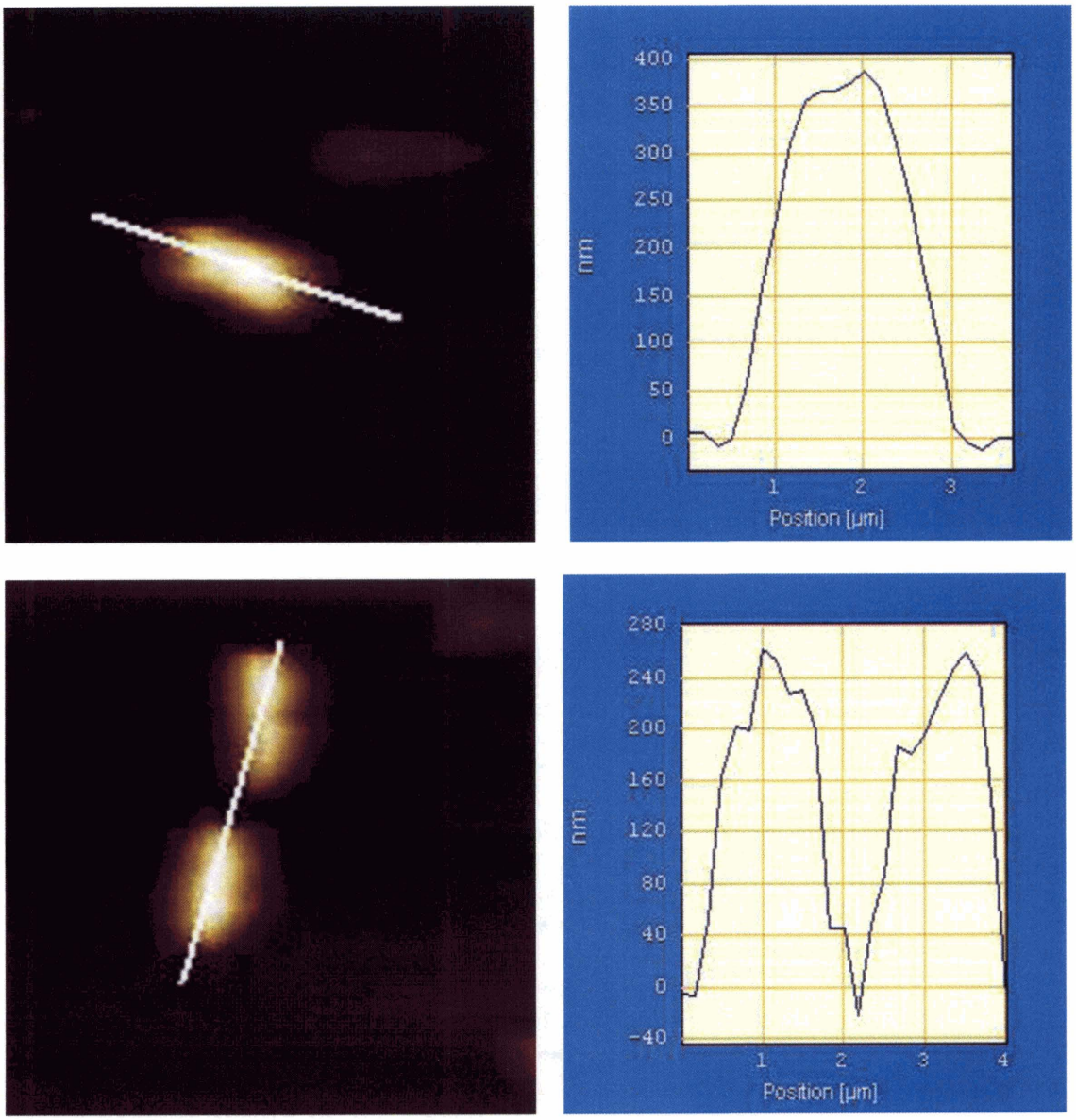

Figure 14. Unlysed *C. necator* Cells Topography and Line Profile.
Magnified topography images of unlysed cells circled in Figure 12 (right) and corresponding line profiles (left). The topography data demonstrates the rod-like nature of the objects; akin to *C. necator* morphological structure as observed with TEM (55). The long axis of these objects is 2µm in length, as measured by line profile data. Based on the object morphology and dimensions, it is concluded that these objects are unlysed cells.

Inclusions were observed to be aggregated together (Figure 13), while other objects looked like whole *C. necator* cells or cell debris. The whole cells are the long oval shaped objects with a length of approximately 2 um in Figure 13 and 14 above. It was concluded that the sonication protocol used was causing incomplete lysis, and the filtration to remove the cell debris enriched these unlysed cells. Aggregation and incompletely lysed cells made this procedure inadequate for the purification of PHB inclusions.

Based on these findings, enzymatic lysis was used to break the cells. Lysozyme is an enzyme that degrades the peptidoglycan outer membrane coating of bacteria. Post lysozyme addition of a high salt concentration creates an osmotic pressure on the bacterial phospholipid bilayer, which is followed by an osmotic pressure in the opposite direction when the cells are diluted in PBS. These osmotic forces help break open the phospholipid bilayer, underneath the bacterial petidoglycan outer membrane. This lysis was observed with fluorescent microscopy and the data are shown below.

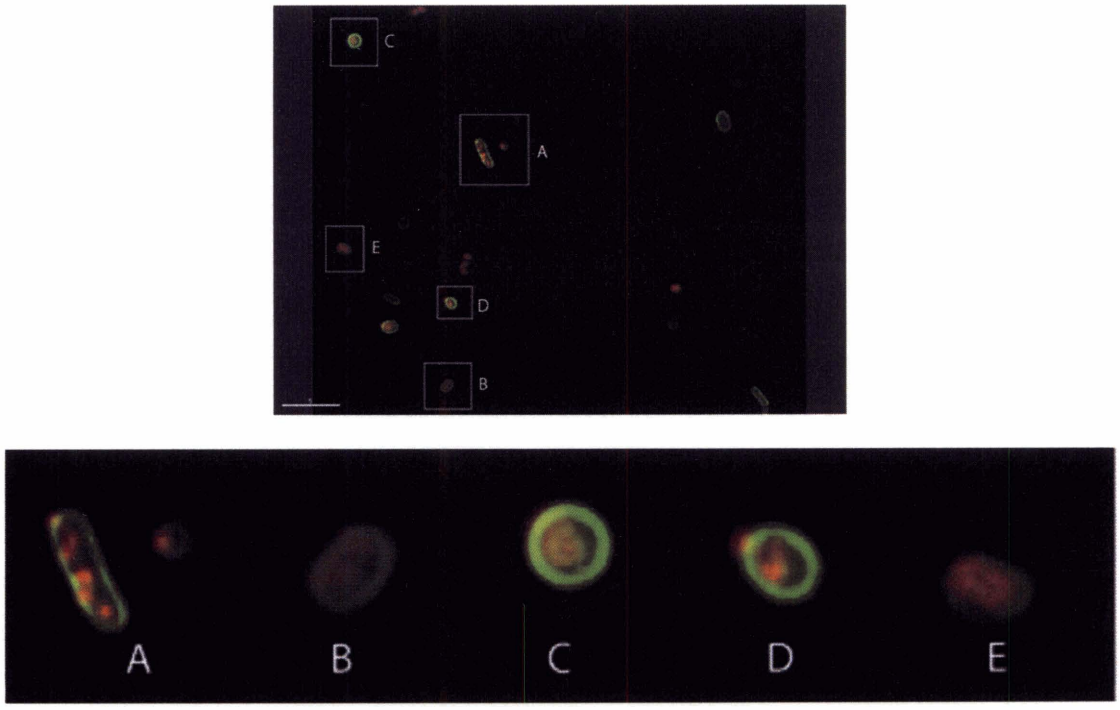

Figure 15. Nile Red and DiO Fluorescent Stain of *C. necator* Whole Cells.
PHB accumulating *C. necator* were cultured and then imaged with fluorescence microscopy (top). Scale bar: 5μm. Individual cells from the top image have been magnified A,B,C,D,E (bottom). The PHB accumulating intracellularly is stained with Nile red, and the bacterial membrane is stained green with DiO as expected.

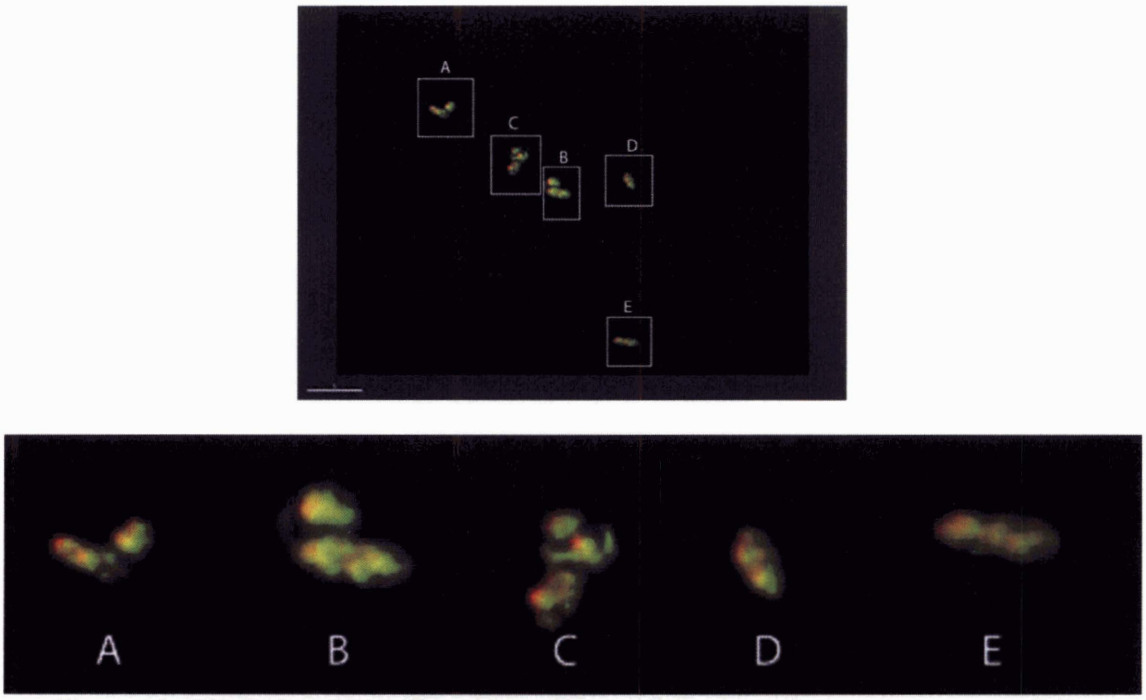

Figure 16. Nile Red and DiO Fluorescent Stain of Enzymatically Lysed *C. necator* Cells. PHB accumulating *C. necator* were cultured and lysed using salt enzymatic lysis (top). Scale bar: 5μm. Individual objects from the top image have been magnified A,B,C,D,E (bottom). The objects are stained with both Nile red and DiO (green), indicating that they are lipophilic. As PHB is the most abundant lipophilic structure in *C. necator* culture in this experiment, the objects are presumably PHB. That fact that PHB is stained with both dyes indicates that complete lysis is occurring. By comparing the objects to the scale bar in the top image, the size of the objects is estimated to be 1 – 3 μm. Additionally, the objects seem irregular in shape. The large size and irregular morphology of the objects indicate that the PHB is aggregating.

Nile red is a low molecular weight lipophilic dye that can penetrate cell membranes and stain hydrophobic objects, whereas DiO is a long ampiphilic dye that cannot penetrate through cell membranes. Therefore, when cells are intact the DiO will stain the membrane of the bacterial cell, whereas the Nile red will stain the inclusions. However, when the membranes have been damaged the DiO's long C_{18} hydrocarbon chain will have an affinity towards lipophilic objects. This results in staining of the inclusions by both DiO and Nile red when effective lysis takes place. The fluorescence microscopy results indicate that effective lysis was taking place, as both the Nile red and the DiO were able to stain the same objects in the lysed cell sample, but not in the whole cells.

However, aggregation was still taking place to some extent in these samples, which is indicated by the size, which are larger than individual inclusions that have diameter of 200 – 500nm under PHB_H growth conditions (1). The reason for this aggregation can most likely be

attributed to the use of salt concentrations to break apart the phospholipid bilayer due to osmotic pressure. PHB inclusions are hydrophobic and thus have a natural tendency to aggregate in the cell. However, remarkably they exist as distinct granules. TEM evidence of coalescence of inclusions is shown when the bacteria have been growing under PHB_H conditions for long periods of time (55). Such conditions were not used in this study, therefore intracellular coalescence is not expected.

The natural affinity of the inclusions to aggregate is thought to be prevented by the presence of the PhaP or phasin proteins that coat the outer surface of the inclusions (19),(38). The mechanism of this stabilization of the inclusions within the cell could be due to surface charge repulsion, which is created by the protein/phospholipid layer on the surface of PHB inclusions. Zeta potential measurements conducted in this study, confirm that the purified granules have a negative surface charge. The addition of salt shields the negative charge on the inclusion surface. Thus the original electrostatic repulsion that exists between native inclusions can be shielded by the addition salt. As the electrostatic repulsion forces decrease, the van der Waals attractive interaction may favor the aggregation of the inclusions. The intermolecular forces between inclusions can be calculated using the following equations: (15):

Equation 1. Lennard-Jones Potential.

$\mathbf{W(D) = -A/D^6 + B/D^{12}}$
A, B = Material Constants ($J\ m^6$)
D= Separation Distance = $1 \times 10^{-9} - 100 \times 10^{-9}$ m

Equation 2. Van der Waals Attractive Force.
For two spheres of equal radii derived from the attractive component of equation 1.

$\mathbf{F(D) = AR/12D^2}$
F = Force (N)
A= Hamaker Constant = 10^{-19} J
R = Radius of Sphere (m) = 250×10^{-9}m
D = Separation Distance (m) = $1 \times 10^{-9} - 100 \times 10^{-9}$ m

Equation 3. Electrostatic Repulsion Force

$F(D) = ((4A\sigma^2)/\varepsilon)e^{-KD}$
F = Force (N)
A = Area of Contact (m^2) = 1.96 X 10^{-13} m^2
σ = surface charge density (C/m^2) = -0.0025 C/m^2
ε = permittivity constant = 7.08 X^{-10}
K = Debye length = 0.1 X 10^{-9} m^{-1}
D = separation distance = 1 X 10^{-9} – 100 X 10^{-9} m

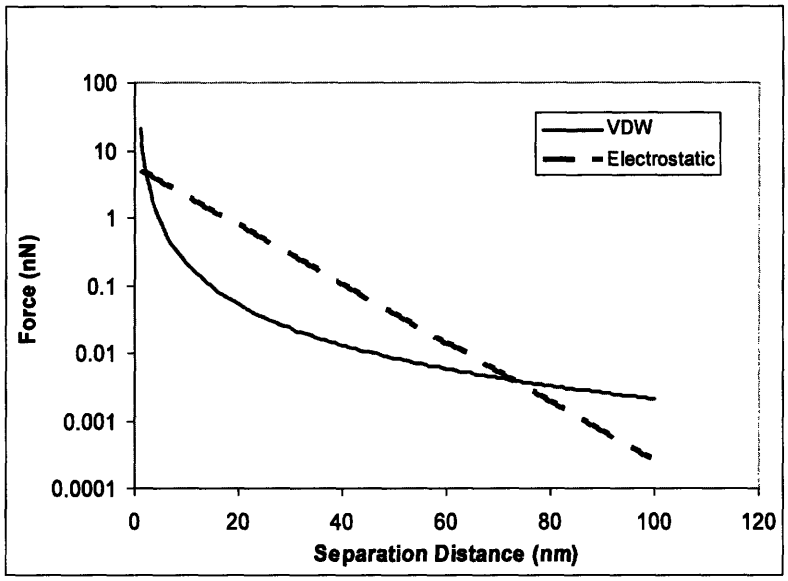

Figure 17. Model of Intermolecular Force Between Two PHB Inclusions.

The calculations indicate that electrostatic repulsion is greater than van der Waals attraction at the separation distances less than 70nm, this may provide repulsion effects to prevent granules from aggregating. When salt is present it can render the electrostatic repulsion ineffective through shielding, thus causing the van der Waals attractive forces to dominate the interaction.

Therefore, enzymatic lysis avoiding the salt was selected as the procedure in this study in order to minimize shielding of the natural electrostatic repulsion between inclusions. A procedure involving a freeze thaw, followed by vortexing, in combination with lysozyme lysis was examined. The results are shown in the Figure 18. A large population of round objects can be observed. These objects are presumed to be inclusions due to the lipophilic staining of the

objects. Additionally, the diameter of the objects falls in the range of what is the expected diameter of PHB inclusions based on TEM images (55). Moreover, a minimal amount of large coalesced objects were observed. AFM images were collected of these granules, which also showed the least number of coalesced inclusions among all the procedures used thus far. The results of the AFM experiments are shown later in this section.

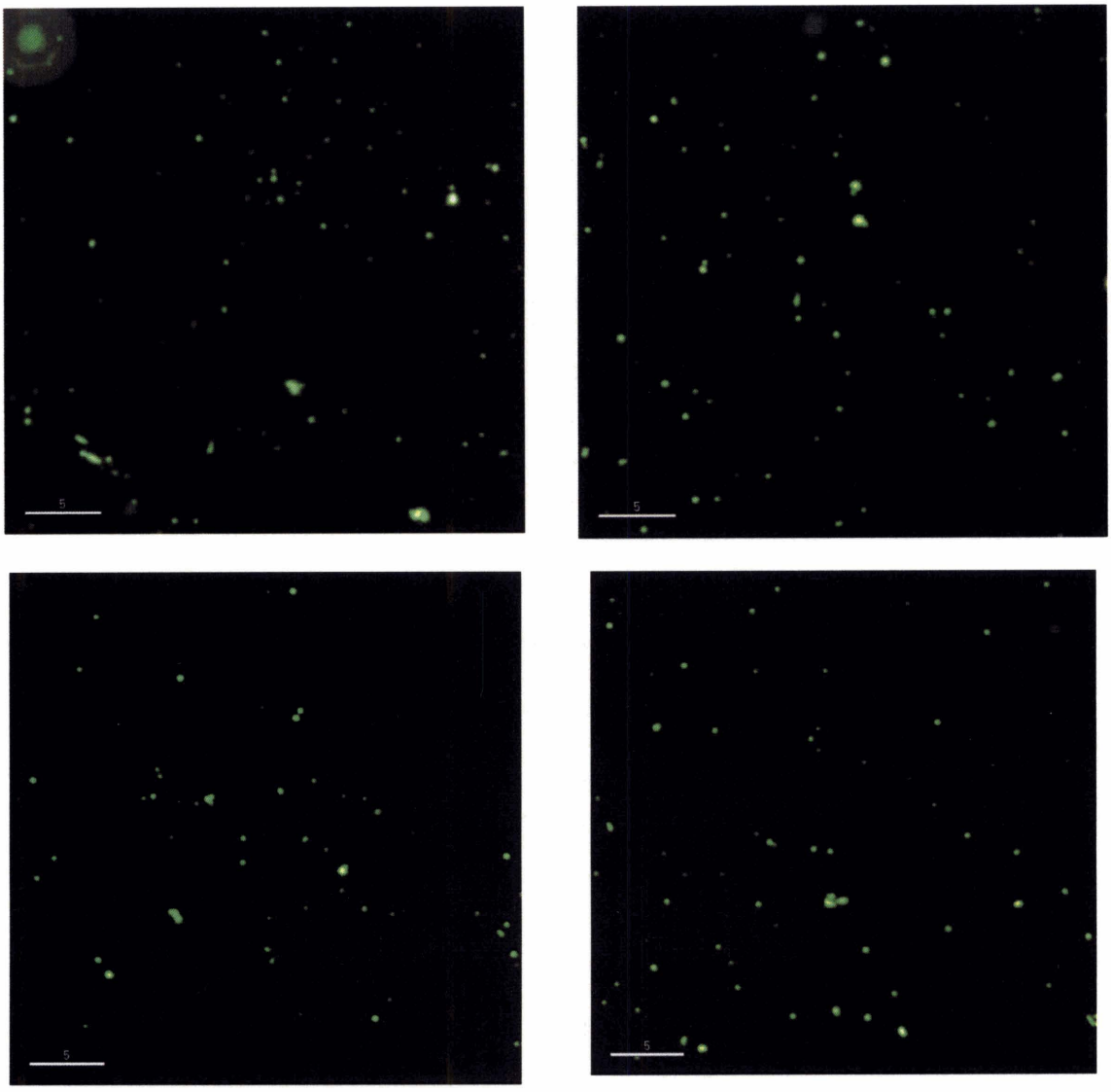

Figure 18. Salt Free Enzymatic Lysis of *C. necator* Followed by DiO Staining. Scale Bar: 5μm.

The salt-free enzymatic lysis appears to be a suitable method to obtain PHB inclusions from in native form from *C. necator*. The enzymatic lysis procedure was best suited for obtaining AFM and fluorescence microscopy images of the PHB inclusions.

The granules prepared using this enzymatic lysis protocol were put through a discontinuous sucrose density gradient ultracentrifugation. The ultracentrifugation resulted in two distinct bands, one at the 1.19 g/cm^3 – 1.22 g/cm^3 density interface, and another at the 1.22 g/cm^3 – 1.26 g/cm^3 density interface. A lighter band was seen at the 1.16 – 1.19 g/cm^3 density interface when large amounts of cell lysate was loaded onto the gradient (Figure 19). These results demonstrate that PHB inclusions are present in a range of densities, varying between 1.16 – 1.26 g/cm^3. Horowitz and Sanders showed that amorphous granules had a density of 1.17 – 1.18 g/cm^3, whereas crystalline PHB had a density of 1.245 g/cm^3 (14). The aim of this study was to examine amorphous PHB granules, and therefore out of the two prominent bands, the 1.19 – 1.22 g/cm^3 density band was collected for characterization. The 1.16 – 1.19 g/cm^3 band could not be analyzed, despite falling in the amorphous density range, because of the low amount of PHB present (For theoretical understanding of PHB density see sections 3.4.2, 3.4.3).

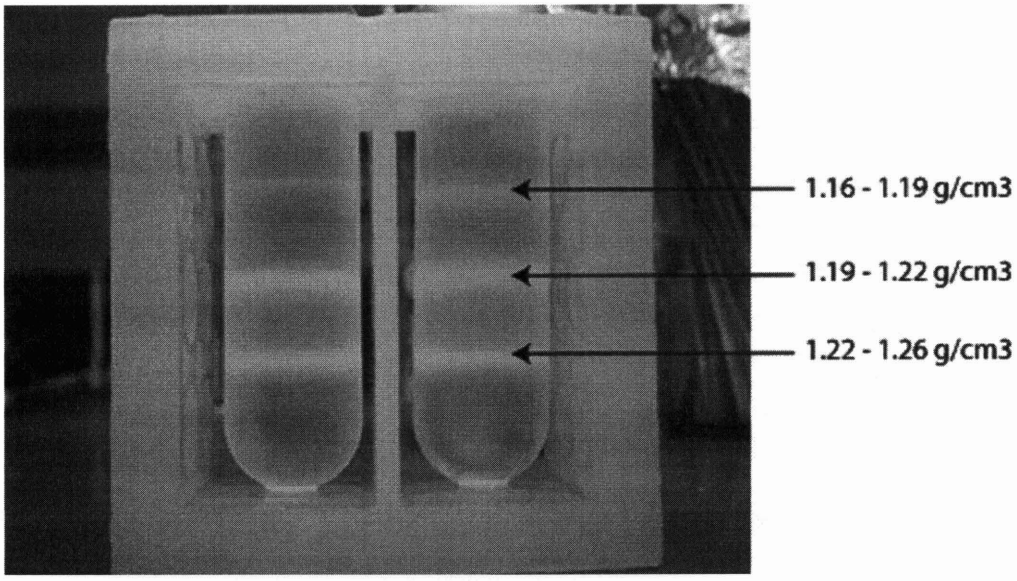

Figure 19. PHA Sucrose Density Gradient Showing Two Prominent Bands.

3. 2. CHARACTERIZATION OF PHB INCLUSIONS

Purified PHB inclusions were characterized using elemental analysis, SDS-PAGE, ^{13}C NMR, western blotting and zeta potential. These analyses were used to determine whether the isolated inclusions resembled native PHB granules. In particular, the amorphous state, the protein content, and the surface charge of the isolated inclusions were examined and compared with expected results. The data gathered from these characterization studies and published literature was used to formulate a model for the native structure of PHB inclusions.

An elemental analysis of the purified PHB inclusions is given in Table 1. Elemental analysis is used determine the presence of elements as a percentage of sample dry weight. The data obtained is compared to what is expected for pure PHB and PHB inclusions. The surface of the PHB inclusions is thought to be covered with proteins, the most abundant of which is the phasin (PhaP) (19),(58). The PHA synthase (PhaC), the negative regulator of PhaP (PhaR) and the intracellular depolymerases (PhaZi) are other proteins thought to be associated with the granule surface (38). Western blotting data has quantified the molar ratios of PHB: PhaC and PhaP: PHB to be 60:1 and 2:1 respectively (53). Using these molar ratio numbers as an estimate of the elemental composition of protein (40% C, 10% H, 25% N, 25% O), an elemental breakdown for PHB inclusions with the associated proteins is calculated (Table 1). The elemental analysis results indicate excess proteins purifying with the inclusions, since the nitrogen content in purified inclusions is greater than expect values based on calculations.

Table 1. Elemental Analysis.

Element	Purified Inclusions (Experiment 1)	Purified Inclusions (Experiment 2)	Pure PHB (calculated)	PHB inclusions with associated proteins (calculated)
C	53.29%	53.29%	56.00%	55.4%
H	7.09%	7.20%	5.80%	6.0%
N	4.35%	4.45%	0%	1%
O	34.15%	34.05%	37.60%	37.1%
S	0.25%	0.23%	0%	0%

SDS PAGE gel analysis was conducted to compare the protein banding pattern of unlysed cells to that of lysed cells and purified inclusions. The results of this analysis supported the conclusion that a large number of proteins were purifying with the inclusions. In particular a large amount of a low molecular weight protein (14kDa) seemed to be a major component of both the cell lysate and the purified inclusions. This was unexpected, as the phasin or PhaP inclusion surface protein (20 kDa), is the smallest molecular size granule associated protein (11). Additionally, the SDS-PAGE results showed little difference between the protein banding patterns of the lysed cells versus the unlysed cells. After analyzing these results it was hypothesized that the lowest molecular weight protein appearing the in SDS-PAGE gel was lysozyme, since the dialysis tube molecular weight cut off is 10 kDa. The reason for co-purification could not be explained by sedimentation rate.

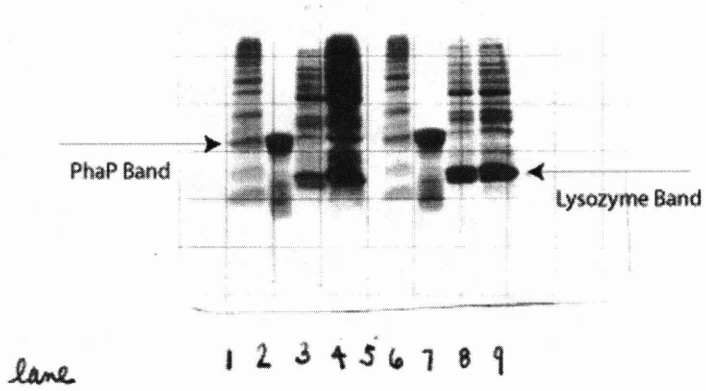

Figure 20. SDS PAGE of Analysis of Protein in Samples.
(1) MW Standard, (2) PhaP Standard, (3) cell lysate, (4)10X concentrated cell lysate, (5) blank, (6) MW Standard, (7) PhaP Standard, (8) 10X PHB inclusions, (9) 50X PHB inclusions

One possible explanation for these results was that the sampling technique (pipetting supernatant and retrieving interface layer of inclusions) was introducing particles from other layers into the sample. This experiment was repeated using an alternative sampling technique, in which a syringe was inserted directly into the layer of interest. The results of this technique are shown below, and clearly indicate that the lysozyme and the other cellular proteins are eliminated from the sample. Additionally, the purified inclusion sample appears to be enriched for PhaP, as can be seen by comparing the molecular weight standard to the protein banding

pattern of the purified PHB inclusions. There is also another prominent high molecular weight band co-purifying with the inclusions, but this protein has not been identified in this study.

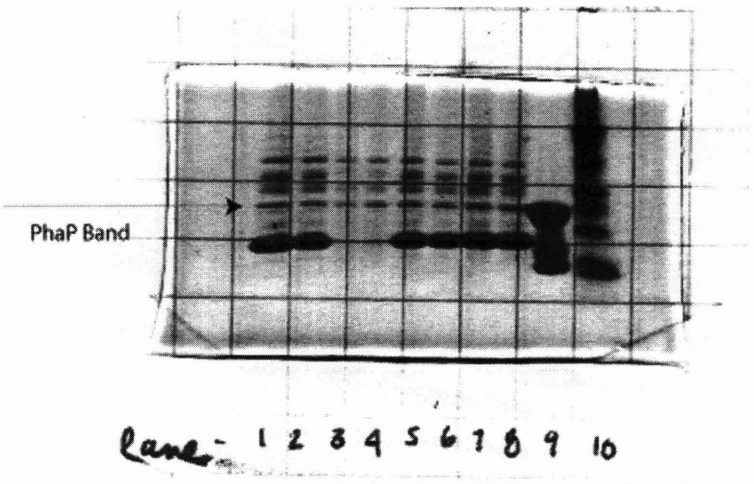

Figure 21. SDS PAGE Analysis of Protein in Samples.
(4) Purified Inclusions (8) Cell lysate (9) PhaP Standard (10) MW Standard

Another granule associated protein that is of interest is PhaC, however, this protein cannot be readily observed in an SDS gel because it is not as concentrated as PhaP. Therefore, western blotting was conducted on the purified inclusion sample in order to determine whether PhaC was co-purifying with the PHB inclusions. The results of this experiment are shown below.

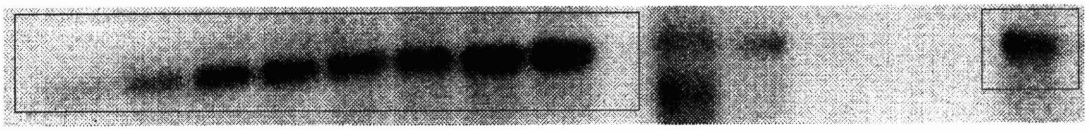

Figure 22. PhaC Quantitative Western Blot.
Left Box: PhaC standard curve in order of least to most concentrated samples (0.5ng, 1.0ng, 1.5ng, 2.0ng, 2.5ng, 3.0ng. 3.5ng, 4.0ng) Right Box: Purified PHB Inclusions.

This quantitative data indicates the concentration of PhaC in the purified PHB inclusion sample, which was calculated as 2.1ng in a 3.75µl of a 10X concentrated inclusion sample. HPLC assay was used to determine the concentration of the PHB in the purified sample, which was 0.758 mgs/ 5ml of inclusion sample. The approximate molecular weight of PHB is around 1000 kDda, and the molecular weight of PhaC is 64 kDa. Based on the concentrations measured experimentally and the known molecular weight of PHB and PhaC, the molecular ratio of

PHB:PhaC was calculated to be 170:1. These results indicate that the purification protocol in use was mild enough to keep at least a certain amount of granule associated proteins (PhaC, PhaP) in association with the inclusions.

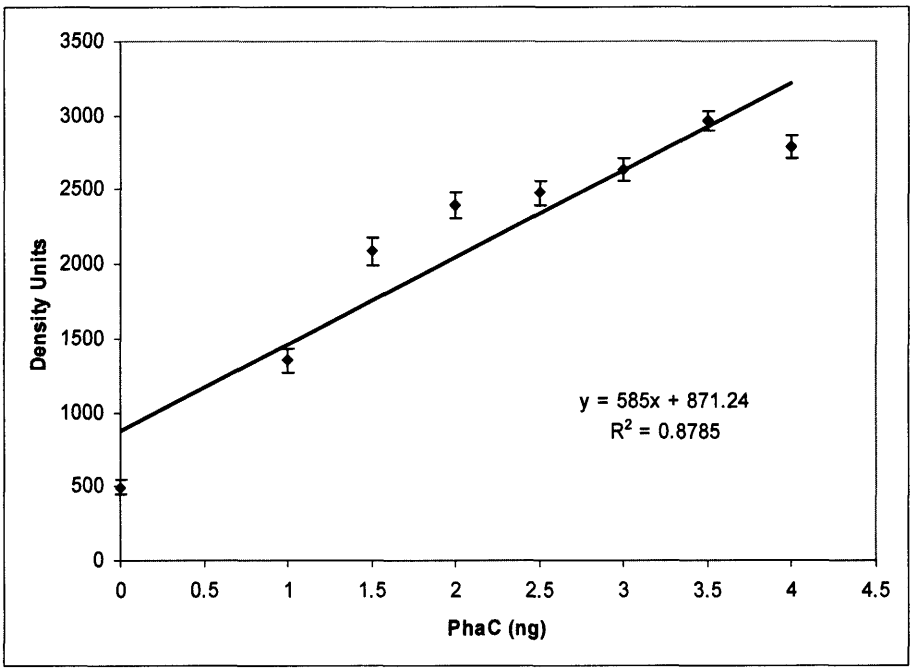

Figure 23. PhaC Standard Curve Based on Quantitative Western Blots.

A distinguishing characteristic of native PHB inclusions, as opposed to purified PHB, is that PHB in inclusion form exists in an amorphous state whereas purified PHB exists in a 60 - 80% crystalline form (1),(56). The isotactic alpha helical structure of PHB can be closely packed forming crystalline structures which have been observed by AFM (13),(34),(52). The inclusion form of PHB retains an amorphous state, due to the activation energy barrier needed to initiate crystallization. As discussed in section 3.4.1. In order to ensure that the purified PHB in inclusions were in an amorphous state, as opposed to a crystalline state, ^{13}C NMR data were collected. ^{13}C NMR can be used to distinguish between solid and liquid states, since solid material does not exhibit a sharp spectrum under normal acquisition conditions (23), (41). Based on the ^{13}C NMR results shown in the figure below, it can be confirmed that the isolation procedure resulted in a population of mobile PHB since a ^{13}C NMR spectrum was observable, and this is in agreement with published work (14).

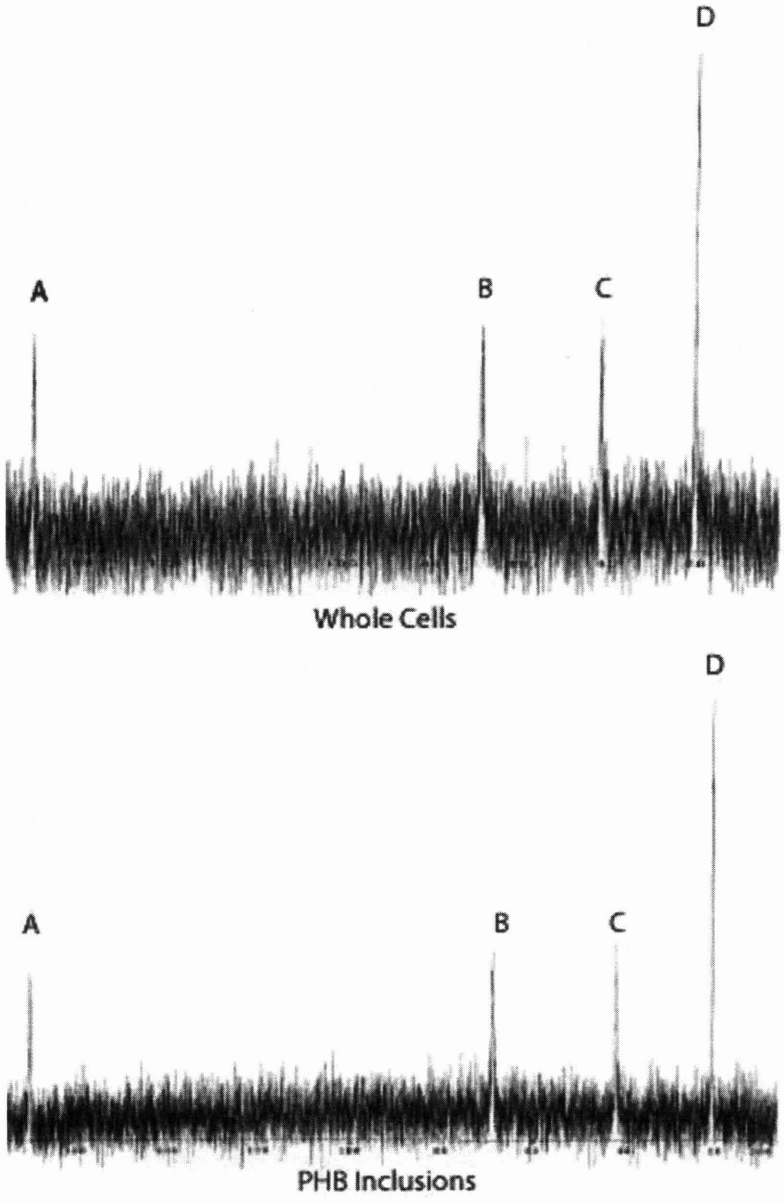

Figure 24. ^{13}C NMR Indicating Amorphous PHB.
Whole Cells (top), PHB Inclusions (bottom). (A) Carbonyl 170ppm, (B) Methine 68ppm, (C) Methylene 41ppm, (D) Methyl 20ppm.

The results of the SDS-PAGE, western blots, and ^{13}C NMR confirmed that the inclusions were co-purifying with both PhaP and PhaC, and were in an amorphous state. Therefore, enzymatic lysis followed by sucrose density ultracentrifugation seemed to be purifying inclusions that resembled native PHB inclusions. Purified PHB inclusions were used in the microscopy studies conducted in the next section.

3.3. ATOMIC FORCE MICROSCOPY (AFM) AND FLOURESCENCE MICROSCOPY TO OBSERVE PHB INCLUSIONS

The PHB inclusions obtained via salt free enzymatic lysis followed by sucrose density ultracentrifugation were used in AFM imaging. As detailed above, prior to AFM imaging we obtained an understanding the amorphous state, protein composition, and aggregation behavior of the PHB inclusions. The purified inclusions were firmly adhered to a glass substrate because movement of the objects decreases the resolution of the AFM imaging. Additionally, the substrate that the sample is placed on is flat in order to reduce background noise.

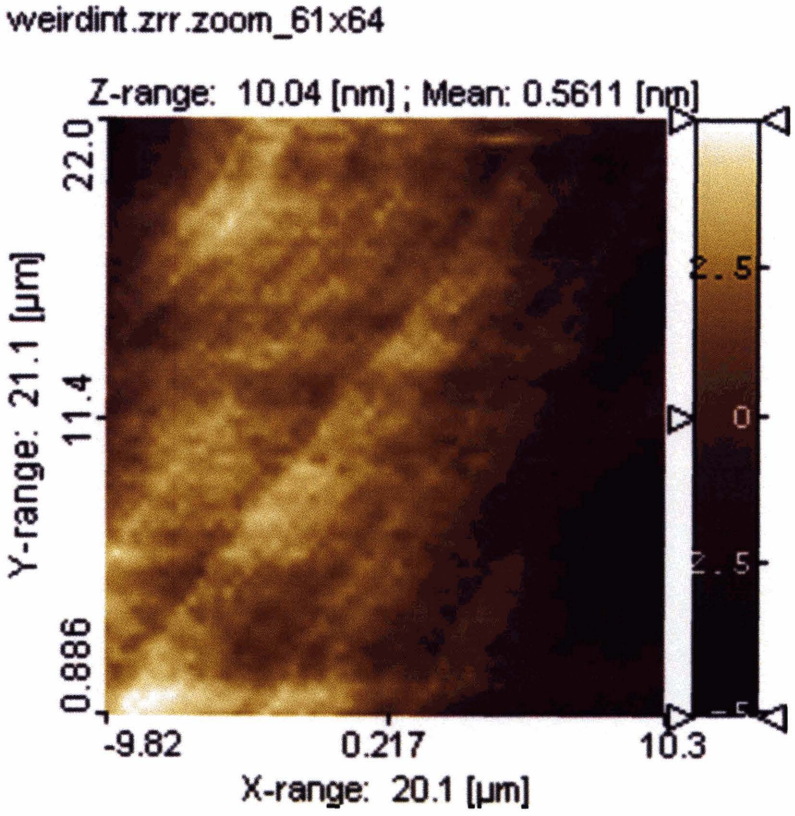

Figure 25. Amino Silane Coated Glass Slide Imaged in Contact Mode Air AFM

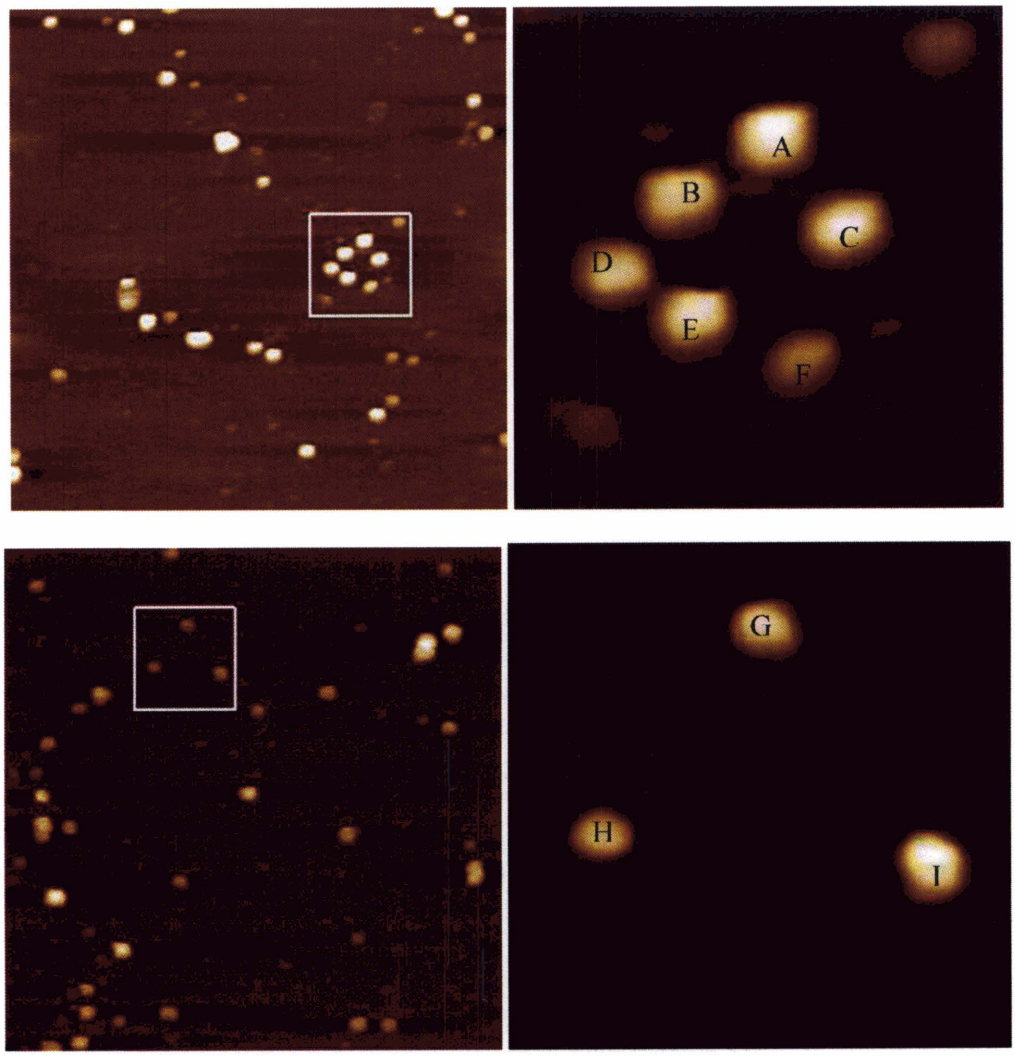

Figure 26. AFM Dry Contact Mode Images of Purified PHB Inclusions.
20 X 20μm Scan Area (Left) Magnified Image (Right). Dimensions of the labeled inclusions on the right are shown in Table 2 below.

Table 2. Dimensions of PHB Granules From Figure 26.

PHB Inclusion	Long Axis (nm)	Short Axis (nm)	Height (nm)
A	670	540	280
B	670	600	230
C	670	600	290
D	540	540	250
E	600	540	260
F	550	400	200
G	600	540	200
H	470	400	220
I	540	540	230

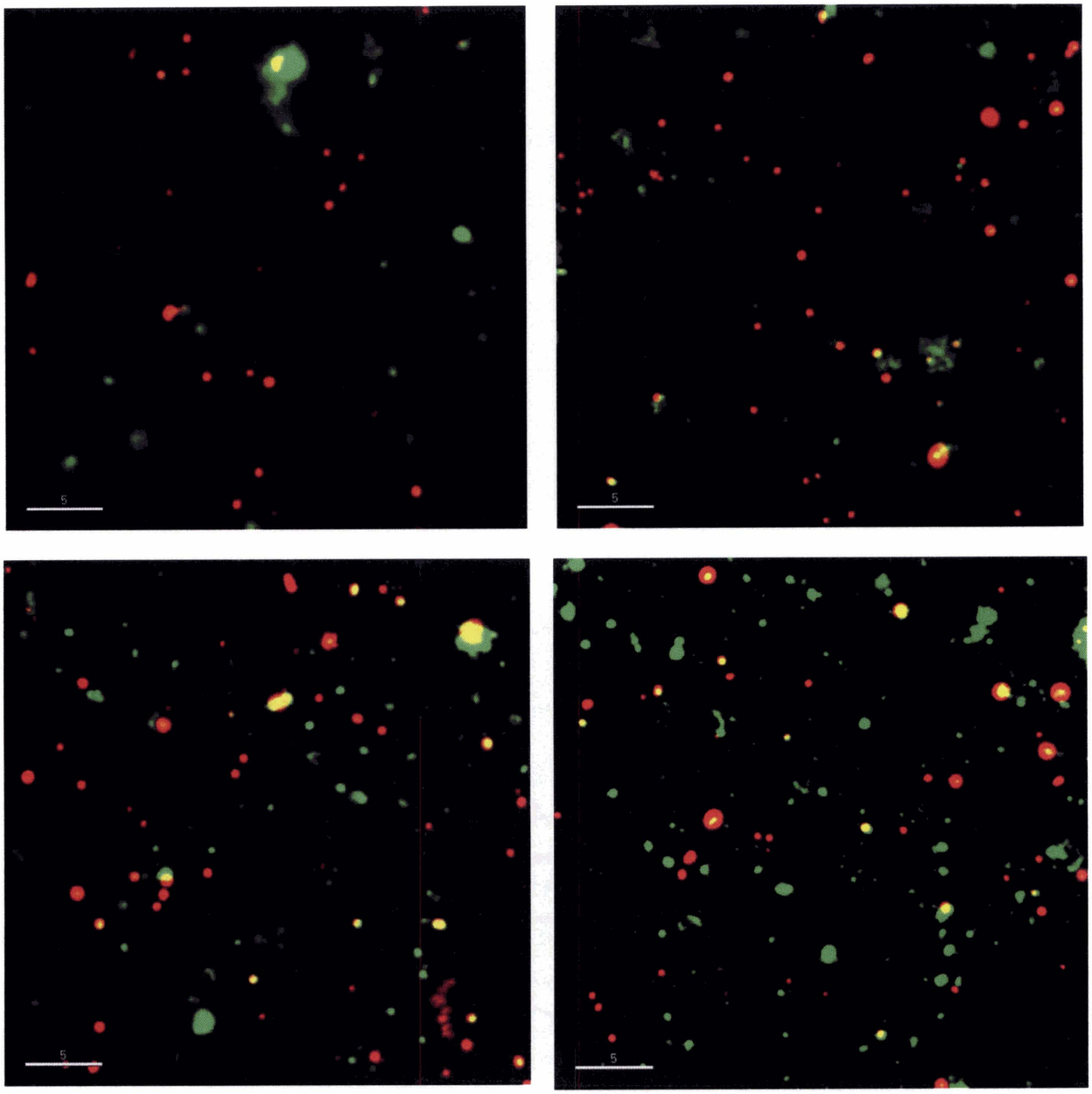

Figure 27. Fluorescently Stained Purified PHB Inclusions.
In the images above PHB Inclusions are stained with lipophilic dyes Nile Red and DiO (green), adhered to an amino silane coated glass slide, and imaged with fluorescence microscopy. Scale Bar: 5μm. The objects stained are unaggregated PHB inclusions, and are similar in size and morphology that observed by TEM measurements**(55)** and AFM measurements conducted in this study.

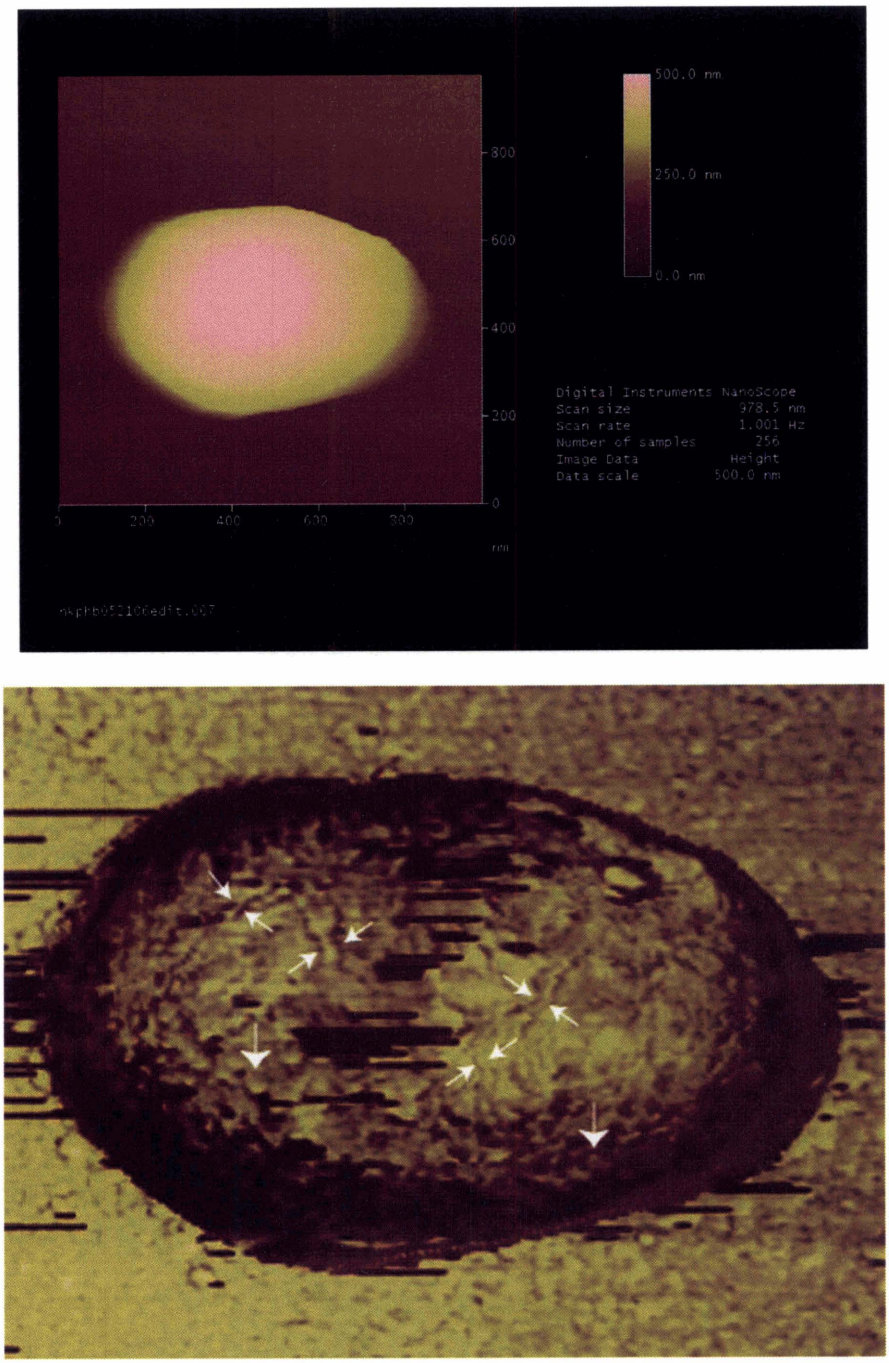

Figure 28. AFM Images of PHB Inclusions Obtained With Tapping Mode in Air.
Topography Image of 1 X 1μm Area (top), Corresponding Phase Image (bottom). Large arrows point to globules and small arrows point to filaments.

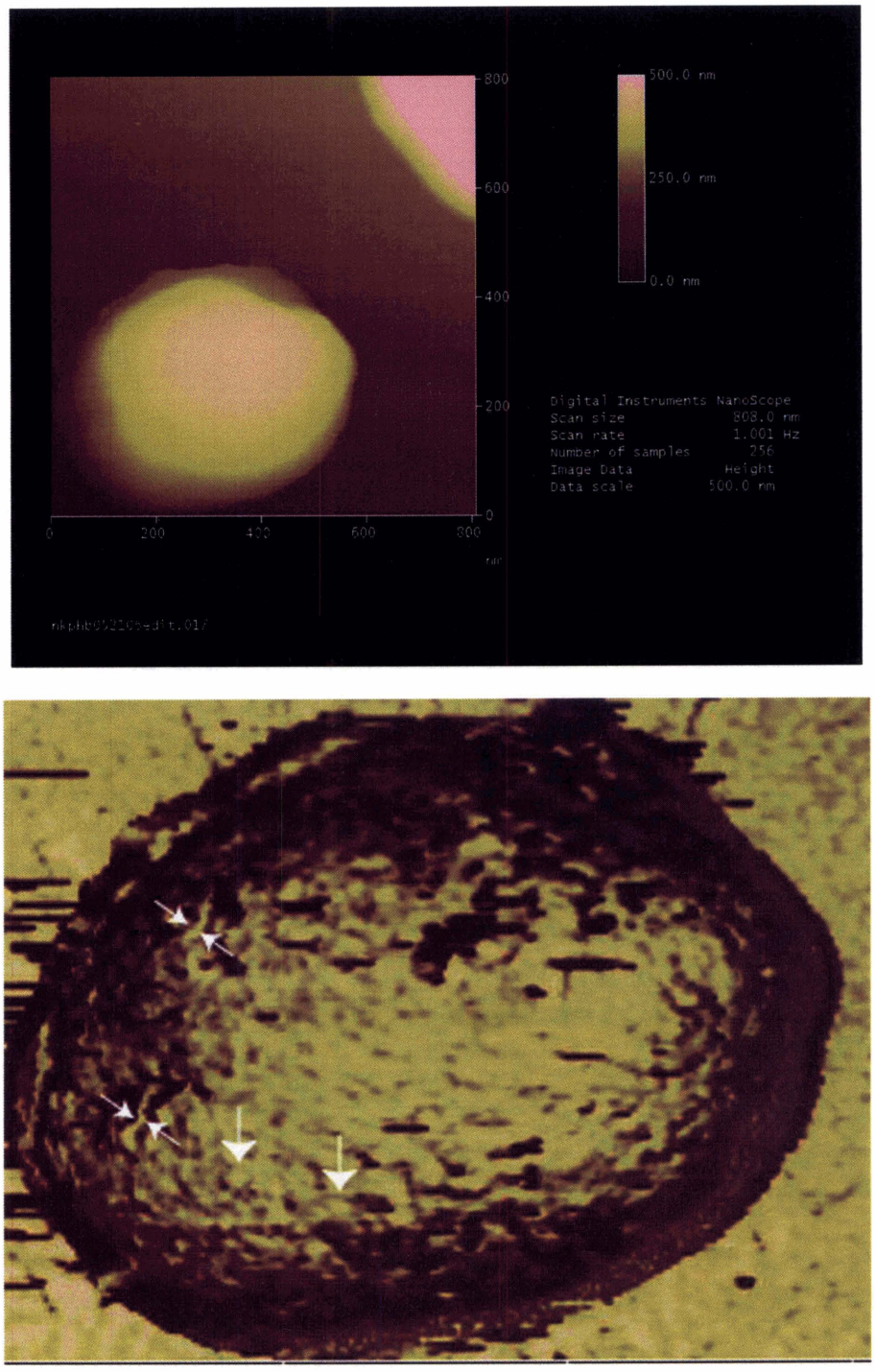

Figure 29. AFM Images of PHB Inclusions Obtained With Tapping Mode in Air. Topography Image of 0.8 X 0.8μm Area (top), Corresponding Phase Image (bottom). Large arrows point to globules and small arrows point to strands.

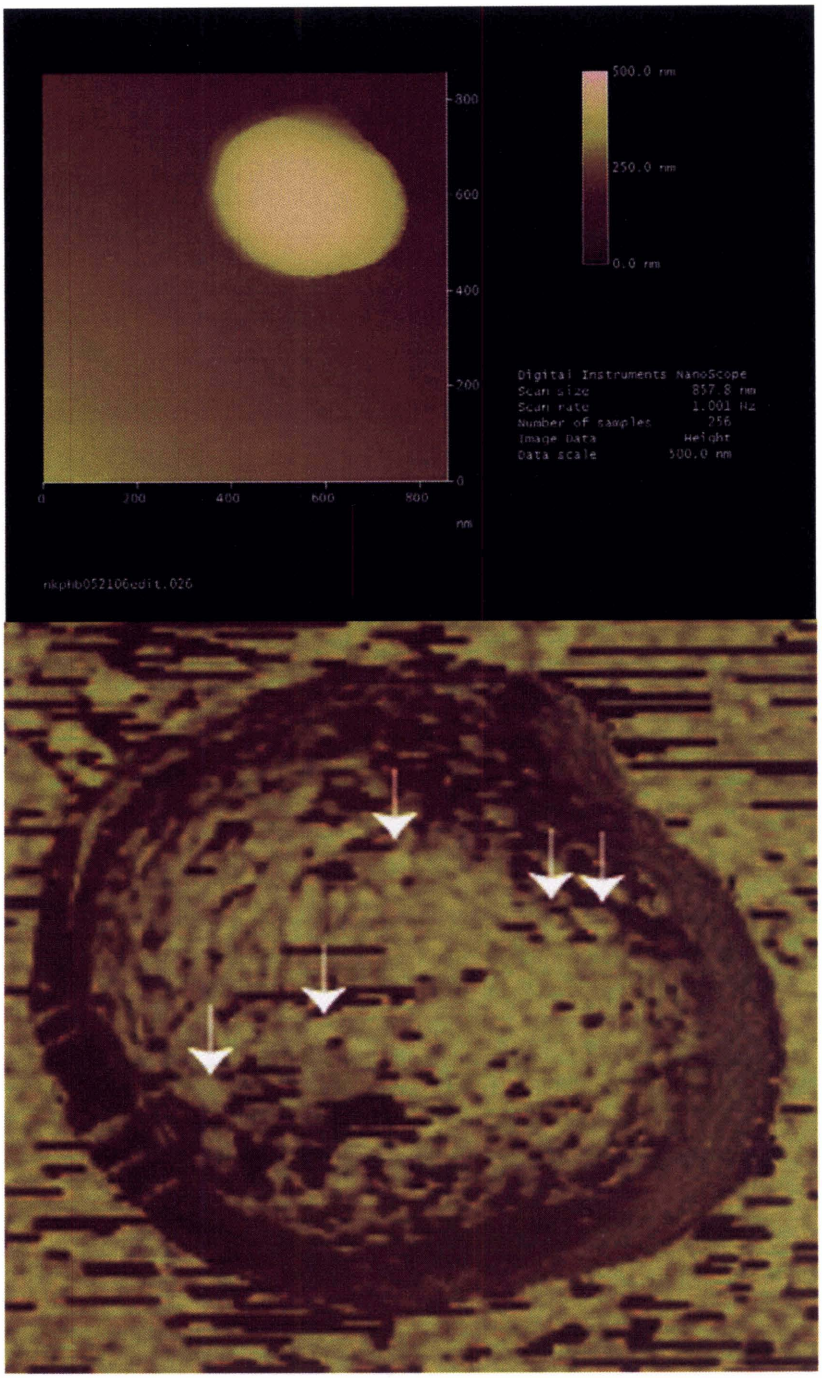

Figure 30. AFM Images of PHB Inclusions Obtained With Tapping Mode in Air.
Topography Image of 0.8 X 0.8μm Area (top), Corresponding Phase Image (bottom). Arrows point to globules.

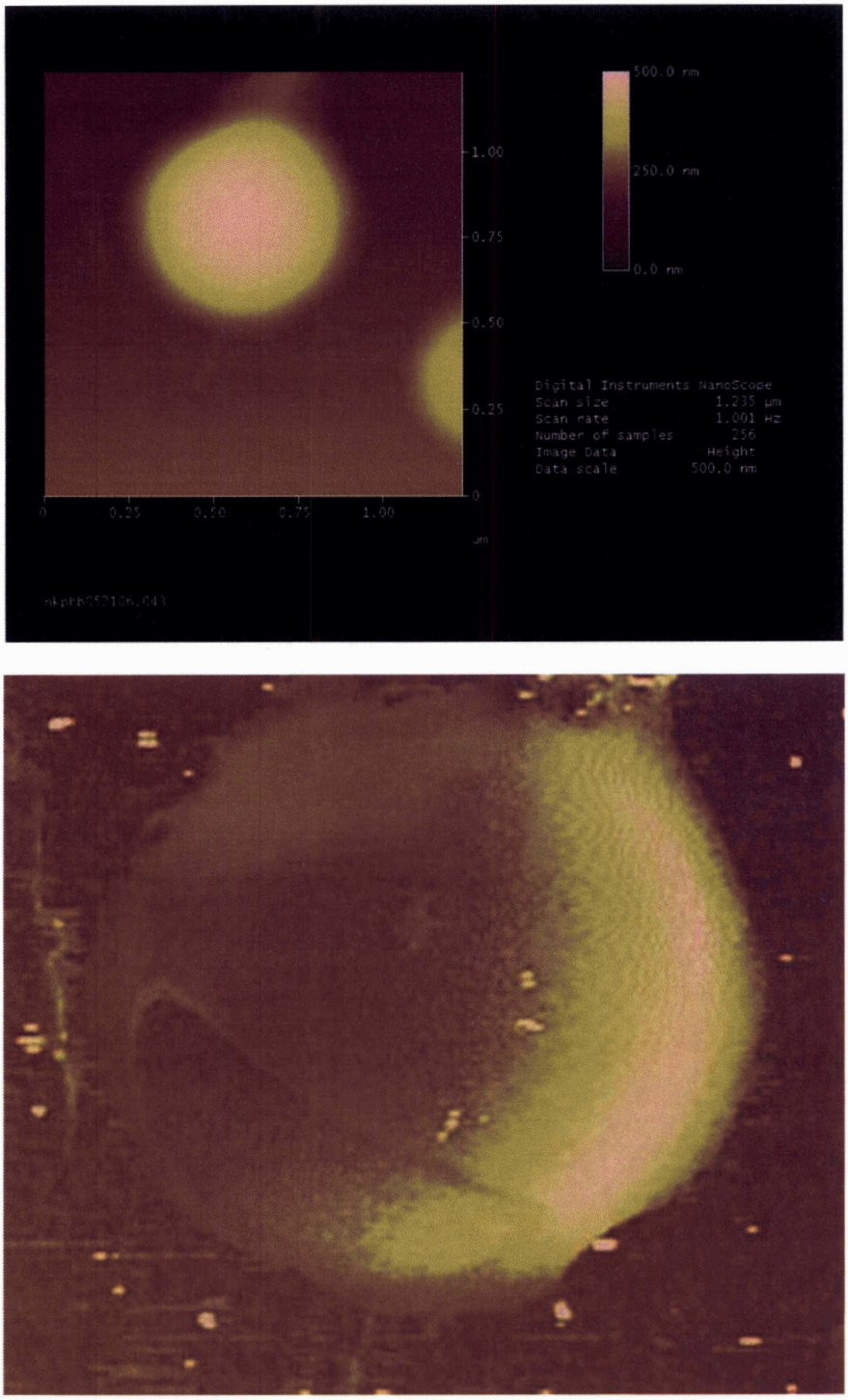

Figure 31. AFM Images of PHB Inclusions Obtained With Tapping Mode in Air. Topography Image (top), Corresponding Phase Image (bottom). Approximately 10% of inclusions imaged showed a smooth surface where no globules could be observed.

In the figures above (Figures 26-31), isolated inclusions were fixed to amino silane coated glass slides via electrostatic attraction. The amino silane coated slides have a positive surface charge, whereas the inclusions have a negative surface charge. Inclusions were incubated with the slide and then the slides were washed in order to remove the residues that were unattached. Finally, the slides are dried and examined using AFM or fluorescence microscopy (for the fluorescence microscopy the isolated inclusions had been stained with a lipophilic dye prior to slide attachment). The image of the plain amino silane coated slide confirms that the roughness of this slide is negligible compared to the objects being viewed. Both the AFM and the fluorescent microscopy show a similar density of round granule-like objects in the view field. This supports the conclusion that the objects being seen with AFM are in fact round lipophilic PHB inclusion bodies. Some of the inclusions observed with AFM were as large as 800μm in diameter, which is greater than the diameter of 200 – 500nm for PHB inclusions often observed with TEM of fixed inclusions (55). The AFM images conducted in this study were done in air, and in published works AFM images of inclusions in air have shown similarly large diameters, perhaps due to some phenomenon associated with inclusion drying (1), (4),(55).

In order to confirm that the objects in the viewfield were PHB inclusions the purified inclusions were analytically examined with HPLC, ^{13}C NMR, and elemental analysis. The data from these analyses confirmed that PHB was present in the purified material. Secondly, AFM and fluorescence microscopy were conducted in parallel. In the fluorescence microscopy, the lipophilic dyes Nile red and DiO were used to stain the inclusions for observation. Under the growth conditions used in this study, no other large lipophilic colloidal object is known to exist in the cells. Both the Nile red and DiO should stain the same objects under ideal mixing conditions. The patchiness of staining observed in Figure 27 is probably due to inadequate mixing. The objects that the lipophilic dyes bind to are presumed to be PHB, due to their lipophilic nature and similarity to the size and shape of PHB inclusions as determined earlier. Both the fluorescent and microscopy results show a similar density distribution of granules, and show minimal aggregation of granules. As such this technique seems like a suitable way to study native PHB inclusions using AFM.

High resolution images of the granules were obtained, and it was shown that most of the inclusions displayed a rough surface topology (Figures 28-30). Some of the inclusions imaged

showed a smooth surface (Figure 31). The rough surfaces of the inclusions were analyzed in order to determine the dimensions of the surface objects. Two types of surface objects were observed: globules and filaments. The globules were the most abundant and are highlighted by the large white arrows. The filaments are less abundant and are indicated by the smaller white arrows. The width of these objects as measured by AFM was determined as 15.7 +/- 5.9nm for the globules and 10.0 +/- 2.7nm for the filaments. However, objects that are approximately the same size or smaller than the AFM probe radius of curvature have exaggerated lateral dimensions when imaged. This exaggeration was accounted for by using an analysis described by Vasenka et al. (57), in which the probe and the scanned objects are represented by hemispheres. The equation from their analysis was used to calculate heights of objects.

Equation 4. Object Width Broadening Due to Tip.

$H = W^2/8R_c$
W = exaggerated object width
R_c = probe radius of curvature
H = actual object height

The probe radius of curvature was supplied by the manufacturer (10nm), and the object width was measured using the phase images. The object height remains the only unknown variable and is assumed to be close to the actual height of the object. The calculated height of the globular objects was 3.1nm +/- 0.4nm and the calculated height of the filaments was 1.2nm +/- 0.1nm. The globules size range that is expected for globular proteins , and the filaments have the height of around two alpha helical chains (34). Additionally, by examining the line profile obtained topography AFM data the average granule diameter was calculated as 550 +/- 100nm.

Table 3. Average Dimensions of PHB Inclusions.

	Long Axis (nm)	Short Axis (nm)	Height (nm)
	740	470	330
	610	480	300
	610	480	310
	590	590	350
	430	390	220
	610	530	250
	440	470	250
	500	590	280
	550	510	440
	550	590	300
	470	430	360
	550	510	180
	750	700	290
	430	550	180
	620	600	380
	630	750	180
	390	510	210
	590	590	350
Average	560	540	290
Standard Deviation	100	90	70

3.4. PROPOSED MODEL FOR STRUCTURE OF NATIVE PHB INCLUSION

Native PHB inclusions resulting from the synthesis and degradation of PHB within the cell are an important component of PHB biosynthesis. By elucidating the physiology of these of unique subcellular structures a better understanding of the structure-function relationship of native PHB inclusions in PHB biosynthesis is possible. In this section a compilation and interpretation of the experimental data in this study and from the literature serve as a basis from which a working model for PHB inclusion structure is proposed. This model represents the current understanding of the nature of PHB inclusions.

3.4.1. Amorphous State of Native PHB

Early X-Ray diffraction experiments conducted on purified PHB polymer, show a distinct pattern associated with crystalline polymer arranged in a helical conformation (27), (5), (30). For a long time it was believed that the polymer existed in this helical crystalline conformation intracellularly, in the late 1980s; however, both ^{13}C NMR and wide angle X-Ray scattering proved to the contrary, and showed that PHB did not confer the crystalline conformation in the native intracellular state (2), (20).

The motivation behind studying the state of the native polymer initially was to understand the irreversible loss of activity of the intracellular depolymerase towards some forms of the isolated polymer. In particular treatments such as freezing and thawing, long-term storage at $4^{o}C$, close packing by centrifugation and drying caused the polymer to become inaccessible to the intracellular depolymerase (31), (32), (10).

In order to reconcile the differences in behavior between treated and untreated polymer, Barnard et al. studied the physical state of the native granules with ^{13}C NMR, and confirmed that the intracellular polymer existed in a totally amorphous state (2). This work led to the start of a new model of native PHB granule structure; not as a close-packed and solid subcellular structure, but as an amorphous and fluid subcellular structure.

In this study ^{13}C NMR technique was used as the basis to determine the state of the isolated PHB inclusions. Under the acquisition conditions used, solids do not give high resolution NMR spectra since their spin relaxation time is much longer than the time scale in which data was collected (23), (41). Since clear peaks are seen corresponding to those expected for PHB, the isolated granules are presumed to be in an amorphous rather than solid state. These results are supported by published PHB NMR studies (14), (2), (46).

3.4.2. Structure and Density of Crystalline PHB

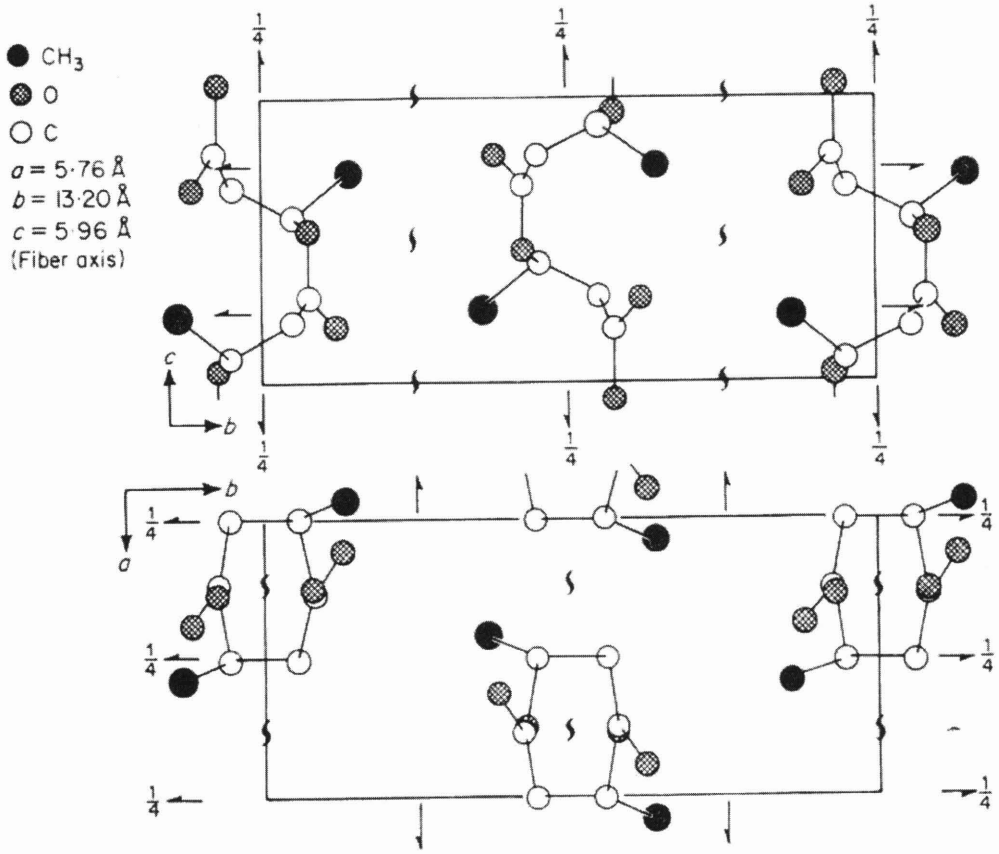

Figure 32. Packing of PHB Chains in Orthorhombic Unit Cell (34).

The crystalline form of PHB exists as an orthorhombic unit cell containing four repeat units from 3 different chains. The unit cell dimensions have been calculated based on X-Ray diffraction data (Figure 32). Based on these dimensions (5.76 X 5.95 X 13.20 Å) and the mass of the PHB repeat units (4 monomers per unit cell), a theoretical density of 1.26g/cm^3 is obtained for crystalline material (34). This is slightly higher than the observed density of crystalline PHB of 1.245g/cm^3 due to the fact that PHB usually exists in around 80% crystalline form (14), (34),(56).

3.4.3. Structure and Density of Amorphous PHB

I modeled the structure of native PHB using the statistical random coil conformation. In this model the lengths of the bonds and the valence angles between bonds are held constant, and are both determined by the chemical structure of the polymer. The rotation around the single bonds can take any value, and as the number of single bonds increases in the polymer, the number of possible states increases exponentially, reaching incomprehensibly large numbers for long polymers such as PHB (6). However, based on a value for the average chain end-to-end distance, the average radius of gyration can be obtained. Assuming that the random coil on average occupied a spherical volume, with a radius equal to the radius of gyration, an estimate for the density of PHB is obtained.

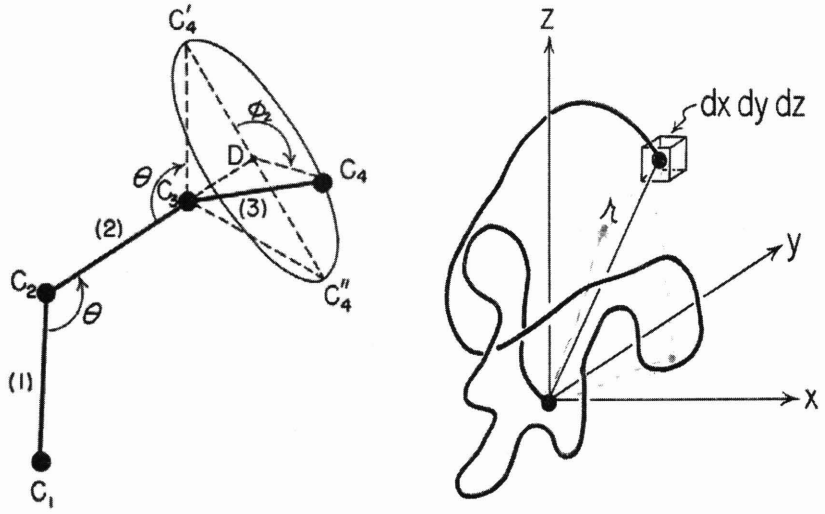

Figure 33. Random Coil Conformation For Polymers (6).
Rotational Freedom Around Single Bonds For Random Coil Conformation (left), Chain End-to-End Distance (right).

There are four single bonds per unit of PHB backbone, and there are approximately 44,000 single bonds (statistical segments) in the backbone of each PHB molecule. Each of these statistical segments has a length of around 1 Å. Based on these numbers, and using the formula for the average radius of gyration, a density is calculated. The equations used are given below:

Equation 5. Chain End to End Distance.

$r = 2/(\pi^{1/2}b)$
$b = \sqrt{(3/(2na^2))}$
n = units per chain
a = length per unit

Equation 6. Radius of Gyration.

$\sqrt{s^2} = \sqrt{(r^2/6)}$
r = chain end to end distance

The theoretical density calculated for amorphous PHB using this formula is 0.67g/cm^3. This is a significant deviation from the values reported in literature and in this study (1.17 – 1.22 g/cm^3). In this simplified analysis, only one chain in isolation was analyzed. However, in reality there are overlaps of many PHB chains in the inclusion space. As chains exist within the same hydrodynamic volume and interact, the density would increase beyond that calculated for amorphous PHB. With overwrap of 1.8 PHB chains the density increases to a value of 1.20 g/cm^3, which is what is observed experimentally for amorphous PHB.

3.4.4. Thermodynamic Energy Barrier to Crystallization

To understand the thermodynamic energy barrier to crystallization it is important to understand the structure of the crystalline unit cell in PHB. PHB alpha helical chains align in an antiparallel fashion, and putative hydrogen bonding can form to stabilize the crystal structure. Based on the unit cell structure of PHB, the hydrogen bonding that seems most likely is between the carbonyl oxygen and a hydrogen from the methyl side chain. This would lead to four hydrogen bonds per unit cell in the crystalline lattice, and these secondary interactions are indicated with dashed lines in Figure 34, and the antiparallel helical conformation presented in Figure 35.

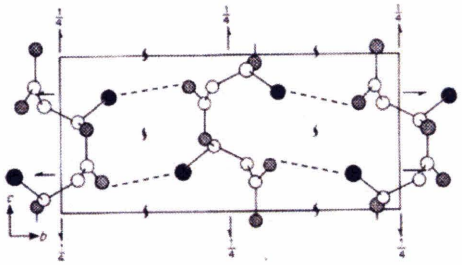

Figure 34. Putative Hydrogen Bonds in a Unit Cell of Crystalline PHB (dashed lines) (34).

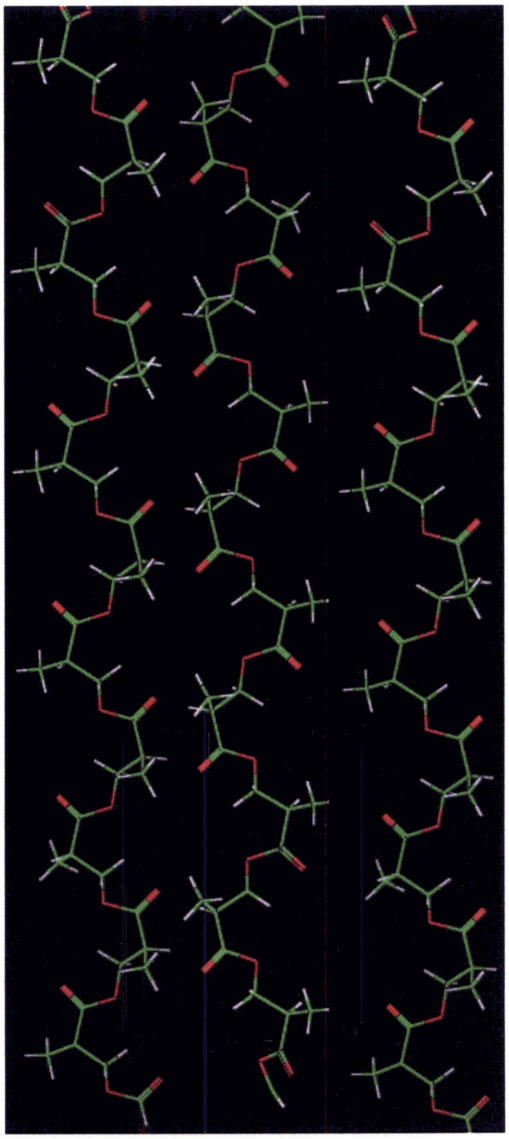

Figure 35. Antiparallel Arrangement of Linear Helical PHB Chains.

A typical value for hydrogen bonds of this type is 1 KJ/mol. Given the long length of PHB chains, even relatively weak secondary interactions can generate high interaction energy density. To crystallize the amorphous random coil polymer, the chain must get from a state of high entropy but low internal energy (amorphous) to a state of low entropy and high internal energy (crystal structure). The higher energy of the crystal structure is due to the hydrogen bonds. For this change to occur, a nucleation event must take place, which would start the onset of crystallization. For the purposes of this study the nucleation event was taken to be the formation of one unit cell in the crystal structure. The activation energy required to start nucleation in PHB was calculated using the equations below (assuming constant T and P):

Equation 7. Gibbs Free Energy.

$\Delta G = \Delta U - T\Delta S$
U = Internal Energy = Hydrogen Bonding Energy
S = Entropy = $N_{monomers}K_B$
K_B = Boltzmann Constant
$N_{monomers}$ = number of monomers in chain

Three PHB chains must come together to form one unit cell, therefore in the thermodynamic analysis only 3 chains are modeled using the following values:

Table 4. Internal Energy and Entropy For Different States of PHB.

State I. Amorphous	State II. Nucleated PHB	State III. Crystalline PHB
U = 0	U = 0	U = 1 KJ/Mol
$S = N_{monomers}K_B$	S = 0	S = 0

Based on Equation 1 and the values in Table 4 the activation energy that must be obtained in order to achieve one nucleation is was derived to be the following:

Equation 8. Activation Energy For Amorphous PHB Nucleation.

Activation Energy = $N_{monomers}K_BT = 1.36 \times 10^{-16}$ J

3.4.5. Nucleation Kinetics of Crystallization

Experimental work with artificial amorphous granules points to the fact that a surfactant-like stabilization layer surrounding the inclusions plays an important role in preventing crystallization of the polymer *in vivo* (14). In particular we see that artificial amorphous granules can be created by emulsifying PHB dissolved in chloroform with the aqueous surfactant cetyltrimethylammonium bromide (CTAB) or the detergent sodium cholate. When these same granules are dialyzed against deionized water, the surfactant coating diffuses down its concentration gradient, thus leaving the granules bare, after which crystallization is observed (14), (46). The results of the artificial granule experiments conducted by Horowitz and Sanders are shown in the figure below.

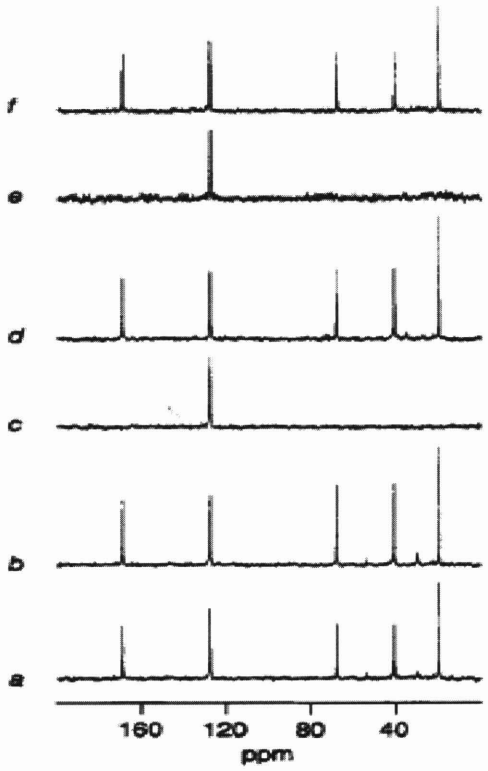

Figure 36 ^{13}C NMR of Artificial Amorphous Granules (14).
(a) artificial amorphous granules coated with CTAB (b) artificial amorphous granules coated with CTAB incubated at 30°C for 11 months (c) artificial amorphous granules coated with CTAB and then dialyzed against deionized water (d) artificial amorphous granules coated with sodium cholate (e) artificial amorphous granules coated with sodium cholate and then dialyzed against deionized water (f) artificial amorphous granules coated with sodium cholate, exposed to soy phospholipids and then dialyzed against deionized water the peak at 127 ppm is due to the internal benzene-d_6 capillary standard.

Based on the experiment conducted on artificial granules, it is apparent that maintenance of the granules as distinct colloid particles is extremely important for preserving their amorphous state. The noncatylitic phasin protein PhaP has been hypothesized to play a role as a biological surfactant for the colloidal stabilization of PHB inclusions.

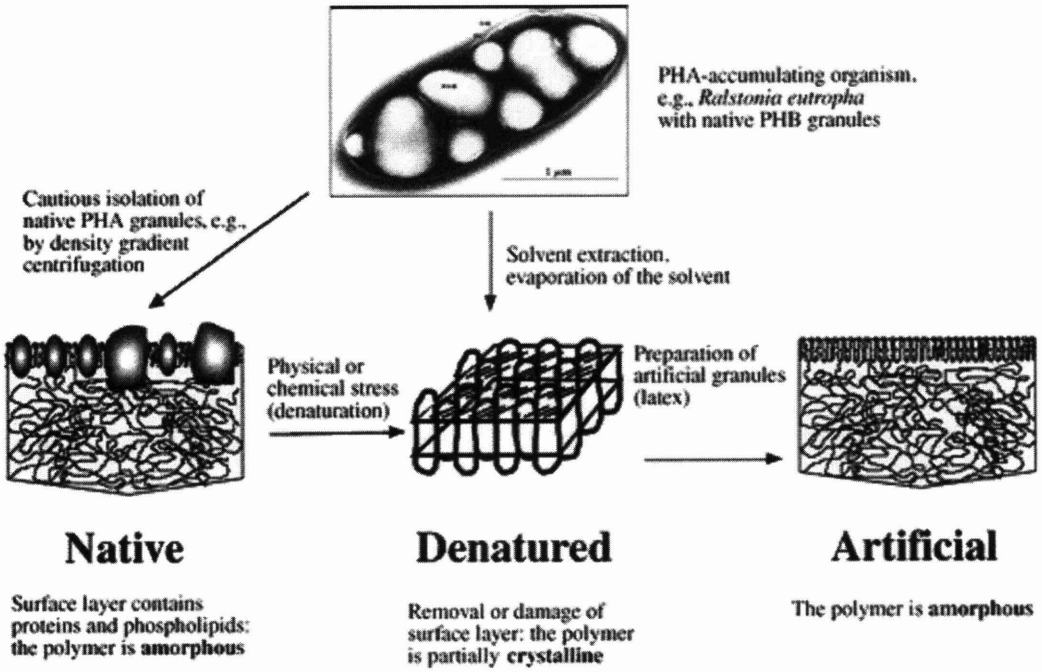

Figure 37. Crystallization of Native Granules in Response to Physical or Chemical Stress or Solvent extraction (16).

3.4.6. PHB Inclusion Associated Proteins

3.4.6.1. PHB Synthase (PhaC)

Four classes of synthases have been identified to date, and more than 59 PHA synthase genes from 45 organisms have been observed (39). Class I synthases create short chain length PHAs, that consist of 3-5 carbon monomeric units (26), (12), (18). Class II synthases create medium chain length PHAs, with 6-14 carbons in each monomer (38), (39). Class III synthases are similar to class I synthases, except they consist of two subunits instead of one (47), (54),

(36). Class IV synthases, have high homology to Class III, but require an activator for synthase activity (38).

C. necator has been the model organism for studying the class I synthase. This synthase (PhaC) was shown to be situated on the surface of PHB inclusions by immunogold labeling (8). Several studies point to the fact that the class I synthase is only active when present as a homodimer, and chain elongation has been hypothesized to take place in the presence of two PhaC active site cysteines (9), (65). The synthase is a 64 kDa protein, and if it is assumed to be a globular it would have a radius of around 3.5nm by comparison to a similar sized protein (Bovine Serum Albumin, 66 kDa) (49).

Each PhaC is responsible for the synthesis of many PHB chains as the enzyme must go through multiple termination and re-initiation steps. A key parameter in understanding the density of this enzyme on the surface of the PHB inclusions is the ratio between the PHB chains and PhaC molecules in an isolated PHB inclusion sample. In this study the number of PHB chains and PhaC molecules in the isolated sample of PHB inclusions indicated by quantitative western blotting was around 170 PHB chains: 1 PhaC. A similar analysis has been conducted by the Tian et al.(53) reports the ratio of PhaC to PHB in a 4 hour *C. necator* culture grown on TSB is 60 PhaC:1 PHB. Additionally unpublished data by the same lab has estimated the amount of PhaC:PHB in a 24 hour PHB_H *C. necator* culture to be 200 PhaC:1PHB(49), similar to the estimates obtained in our study. The results from our study will be used to calculate the amount of PhaC on the surface of the PHB inclusions in the last part of this section.

3.4.6.2. Phasin (PhaP)

PhaP is the most abundant granule associated protein in the cell, and under PHB accumulation conditions represents up to 5% of the total cellular protein content (59), (11). It has been proposed that this protein acts as a natural biological surfactant, coating the outside of the PHB granules, thus preventing coalescence and subsequent crystallization of the granules (38). The presence of PhaP within the cell has a great impact on the size of the PHB inclusions. When PhaP is overexpressed the granules are smaller in diameter than wildtype; whereas when PhaP is not expressed only one large granules exists within the cell (43), (44).

In western blot analyses of the ratio of PHB chains to PhaP molecules of *C. necator* cells grown in TSB for 4 hours, and in PHB_H for 24 hours it was found that around 1-2 PhaP

molecules exist for every PHB chain(53). The size of the phasin protein is around 20kDa, and if it is assumed to be a globular protein then the radius should be around 2.1nm when compared with protein of similar size (chymotrypsinogen A, 25 kDa) (49). In this study PhaP co-purified with the isolated granules at high levels, and could be detected simply by SDS-PAGE followed by Coomassie Blue staining. The ease of detection of PhaP is indicative of the fact that the protein is in high abundance within the cell under PHB_H culture conditions. As with PhaC these results will be used to calculate the amount of PhaP on the surface of the inclusions.

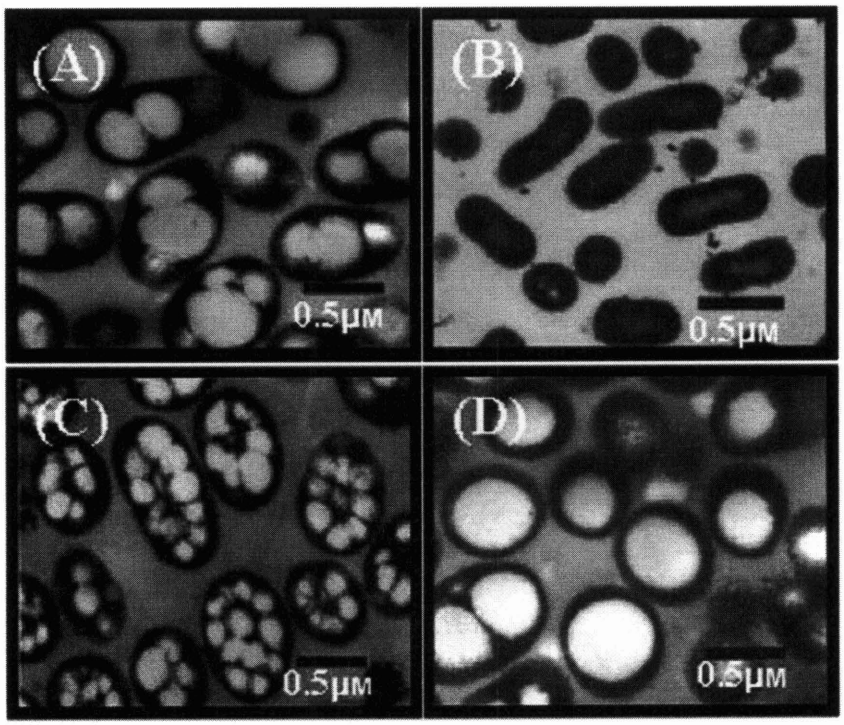

Figure 38. PHA Production as a Function of PhaP Expression (44).

(A) wild type *C. necator* (B) Δ*PhaC* (C) Δ*PhaR*→ over expression of PhaP (D) Δ*PhaP* no expression of phasin (44)

In addition to the PhaP phasin described above, three other phasins have been identified based on homology with PhaP, these homologous proteins are named PhaP2, PhaP3, and PhaP4(37). PhaP2, PhaP3, and PhaP4 have predicted molecular weights of 20.2, 19.5, and 20.2 kDa respectively, and they have been shown to be granule bound; however, they seem to be

expressed at much lower levels in the cell as compared with PhaP and therefore will not be included in this study.

3.4.6.3. Phasin Regulator (PhaR)

PhaR is the negative regulator of PhaP that binds to the upstream region of *pha*P. When PHB biosynthesis occurs, the levels of PhaR are depressed within the cell, thus causing more PhaP to be transcribed (38), (64). PhaR is a 20kDa protein, with a radius of 2.1nm, similar to that of PhaP(49). It has been calculated through western blots and stereological analyses that the ratio of PhaC:PhaR is around 1:2, which translates to a ratio of approximately 85 PHB:1 PhaR based on the PhaC quantitative western results obtained from this study(53). These results will be used to calculate the amount of PhaR on the granule surface.

3.4.6.4. PHB Depolymerases (PhaZ1, PhaZ2, PhaZ3, PhaZ4, PhaZ5) & 3-HB Oligomer Hydrolase (PhaY)

Several bacteria are capable of degrading PHB. PHB is generally released into the environment when polymer accumulating cells die and spill their contents into their surroundings. Bacteria have evolved to excrete extracellular depolymerases and utilize this crystalline form of PHB in their environment (16), (17). Bacteria that secrete extracellular depolymerases, do not necessarily possess the ability to synthesize PHB intracellularly (38).

By contrast intracellular depolymerases can only act upon amorphous polymer, and are only synthesized by bacteria that are able to synthesize PHB intracellularly. PhaY represents 3-HB oligomer hydrolases, which are also involved in breaking down polymer (22), (21).

Just as the PhaC synthase is located on the surface of the inclusions and serves to polymerize excess soluble substrate into insoluble storage polymer, the depolymerases are located on the surface to conveniently degrade the insoluble polymer into soluble substrate when the cell signals it needs carbon and energy. Intracellular depolymerases are not as well understood as extracellular depolymerases (62), (42). However, some work has been done to characterize these intracellular depolymerases. In particular, PhaZ1 has been studied by Tian et. al. who have observed that in *C. necator* cells grown in TSB the ratio of PhaC: PhaZ1 goes from 5:1 at 4 hours to 1:1 at 24 hours (53). The molecular weight of PhaZ1 is 47 kDa and assuming it's a globular protein its radius is assumed to be around 2.8nm based on comparison to a similar

sized protein (ovalbumin 43 kDa) (53). Since in this study, PHB accumulating conditions are used to culture the cells, PhaZ1 along with other depolymerases are probably not being highly transcribed. For this reason the lower ratio of 5 PhaC:1 PhaZ1 (or 850 PHB:1PhaZ1) will be used to calculate the amount of PhaZ1 on the surface of the granule.

3.4.7. PHB Inclusion Lipid Monolayer

Past microscopy studies have revealed what seems like a lipid monolayer surrounding the native inclusions. In Figure 39, electron microscope images compare the thickness of the cellular membrane to the granule membrane (3). The cellular membrane observed as having double the thickness of the granular membrane, leading to the hypothesis that a phosholipid monolayer coats the surface of the granule. Additionally, work analyzing the composition of isolated granules has found that 0.5% (w/w) of the PHB inclusions is composed of lipids (38). However, more work understanding the component of the granule stabilization layer in needed to confirm the presence of lipids on the surface of the granule.

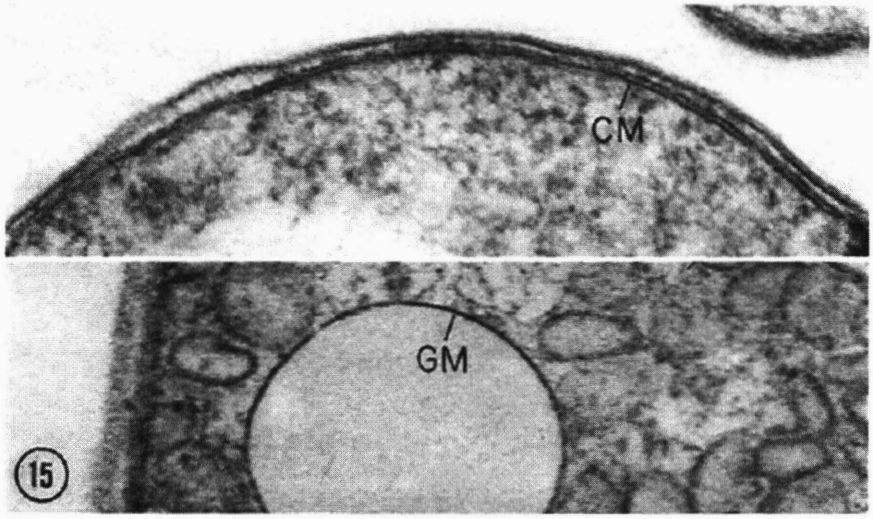

Figure 39. Comparison of PHB granule surface layer and cellular membrane in *Rhodospirillum rubrum* (3).

3.4.8. PHB Inclusion Surface Charge Density

One mechanism by which PHB inclusions are thought to remain as distinct colloidal entities within the cell is via electrostatic repulsion. For electrostatic repulsion to take place, the granules must possess a surface charge density.

Zeta potential experiments conducted in this study revealed that the inclusions have a negative surface charge density (BIC PALS Zeta Potential Analyzer). Dilute amounts of purified PHB inclusions were studied under an electric field, in an aqueous solution of ionic strength I = 0.006. At this ionic strength the Debye length K^{-1} is approximately 10nm. The Smoluchowski equation was used to calculate zeta potential based on mobility measurements since Ka >> 1 (where K is the Debye length and a is the inclusion diameter).

Equation 9. Smoluchowski Equation.

$\mu = \zeta\varepsilon/\eta$
$\mu = v/E$ = electrophoretic mobility
v = velocity
E = electric field
ζ = zeta potential
ε = electric permittivity
η = viscosity

By inserting the electrophoretic mobility value obtained from the experiment into the Smoluchowski Equation, a value of -32.0 mV is obtained for the zeta potential. In order to calculate the surface charge density the linearized Poisson Boltzman equation, along with the parallel-plate capacity model for surface potential were used.

Equation 10. Linear PB Equation with Debye Huckel Approximation.
$\sigma_1 = \varepsilon\kappa\Psi_1$
σ_1 = surface charge density (of inclusion or zeta potential surface)
ε = electric permittivity
κ = Debye length
Ψ_1 = surface potential (of inclusion or zeta potential surface)

Equation 11. Parallel Plate Capacity Model.
$(\Psi_o - \Psi_\delta)/\delta = \sigma_\delta/\varepsilon_\delta$

Ψ_o = inclusion surface potential
Ψ_δ = zeta potential
δ = distance between zeta potential surface and surface of granule
σ_δ = charge density at zeta potential surface (obtained from linear PB equation)
ε_δ = electricity permittivity

Once Ψ_o is calculated, it is applied in the linear PB equation to calculate the inclusion surface charge density, in this case calculated to be -0.00225 C/m^2. This value is equivalent to 1e/70 nm^2, which is the approximate surface charge density on the PHB granule.

3.4.9. PHB Inclusion Mass Density

Based on the results of the ultracentrifugation experiments conducted in this study, the density of the purified PHB inclusions was found to be in the range of 1.19 – 1.22 g/cm^3. This density range is slightly higher than 1.17 - 1.18 g/cm^3 observed by Horowitz et. al. of the PHB homopolymer. Using a middle value of the PHB inclusion density range observed in this study of 1.20g/cm^3, considering that the molecular weight of PHB is 1 X 10^6 Daltons, and that the size of PHB inclusions is between 200nm and 500nm, the number of chains in a PHB granule can be approximated to be between 3000 – 50,000 chains per PHB granule.

3.4.10. PHB Inclusion Structural Model

Based on the work reviewed in this section a model for the structure of native PHB granules is presented. In particular this model will take into account the fact that PHB granules exist as distinct amorphous colloidal structures within the cell, with a stabilization layer consisting of the granule associated proteins PhaP, PhaC, PhaR, and PhaZ1. Superimposed on top of this stabilization layer is the negative surface charge density of the inclusions likely due to the proteins or putative phospholipids.

However, before proceeding with the model, an understanding of the distribution density of each granule-associated protein on the surface of the inclusion should be calculated. Based on the data collected in this study and in published works, the ratio of PHB chains to each granule associated protein of interest was obtained. This value was used to get a number for the proteins present in a 200nm diameter and a 500nm diameter PHB granule, and the results are shown in Table 5.

Table 5. Number of Proteins Per PHB granule.

PHB Inclusion Diameter Size (nm)	200	500
# of PHB chains	3000	50000
# of PhaC molecules 170PHB:1PhaC	20	300
# of PhaP molecules 1PHB:1.5PhaP	2000	30000
# of PhaR molecules 85PHB:1PhaR	40	600
# of PhaZ1 molecules 850PHB:1PhaZ1	4	60

It is assumed that all proteins are globular proteins. The radii of PhaC, PhaP, PhaR, and PhaZ1 are taken to be 3.5, 2.1, 2.1, and 2.8nm respectively (49). The surface area that each globular protein occupies is calculated by the following equation:

Equation 12. Effective Surface Area Occupied by Globular Protein

$$\mathbf{SA\ (protein) = 4r^2}$$

A square is used, rather than a circle to calculate the area occupied by each globular protein, because close packing is assumed. For the purposes of this situation the surface that the

proteins are attached to can be assumed to be flat, as the granule is many orders of magnitude larger than the proteins, and the curvature of the inclusions will not affect the protein close packing.

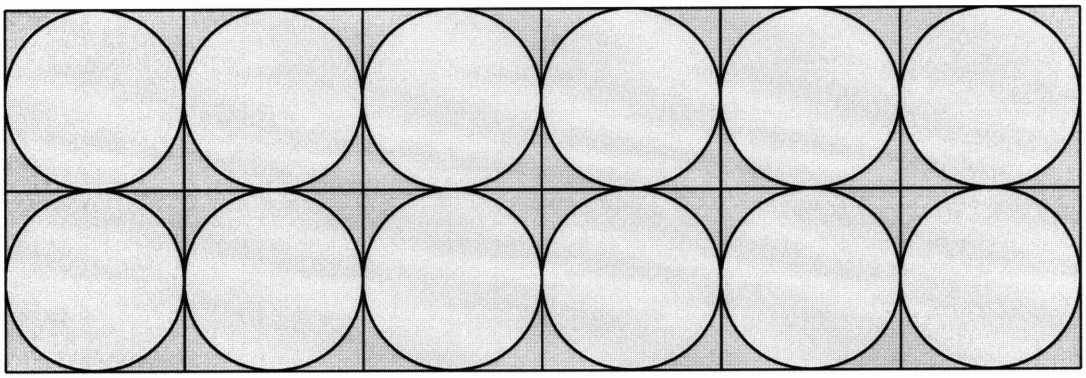

Figure 40. Close Packing of Spheres on a Planar Surface.

By calculating the area occupied by each granule associated protein, and then multiplying by the number of protein molecules associated with each granule (Table 5), we can calculate the percent of the surface of the granules that is covered with each protein was determined. Since volume increases with the cube of the radius, whereas surface area only increases with the square of the radius, the percent protein coverage will become greater as the granules increase in size. The results of these calculations are shown in Table 6.

Table 6. Percent of Protein Coverage on PHB Granule Surface.

	PhaC	PhaP	PhaR	PhaZ1
Radius	3.5 nm	2.1 nm	2.1 nm	2.8 nm
Area Occupied by One Protein	50 nm^2	20 nm^2	20 nm^2	30 nm^2
Area Occupied by protein on Granule of d = 200 nm	900 nm^2	35000 nm^2	600 nm^2	100 nm^2
Percent of total Granule (d = 200 nm) Area Occupied by protein	0.7%	27.1%	0.5%	0.1%
Area Occupied by protein on Granule of d = 500 nm	14400nm^2	590000 nm^2	10000 nm^2	1900 nm^2
Percent of total Granule (d = 500nm) Area Occupied by Protein	1.8%	74.4%	1.3%	0.2%
Average Percent of granule covered by protein	**1.2%**	**50.1%**	**0.9%**	**0.2%**

Based on the calculations above a consolidated model for the surface of PHB inclusions can be obtained, in which the most prominent granule associated protein is PhaP, after which there is PhaC and PhaR, followed by PhaZ1. The spaces in between these proteins contain a phospholipid monolayer. The surface has a charge density of 1e/71nm^2, leading to a total charge of 1830 e to 11100 e (depending on the size of the granule). Underneath the complex stability layer, lies the bulk of the inclusion, which is composed of amorphous PHB polymer. A schematic of this model is shown in the Figure 41.

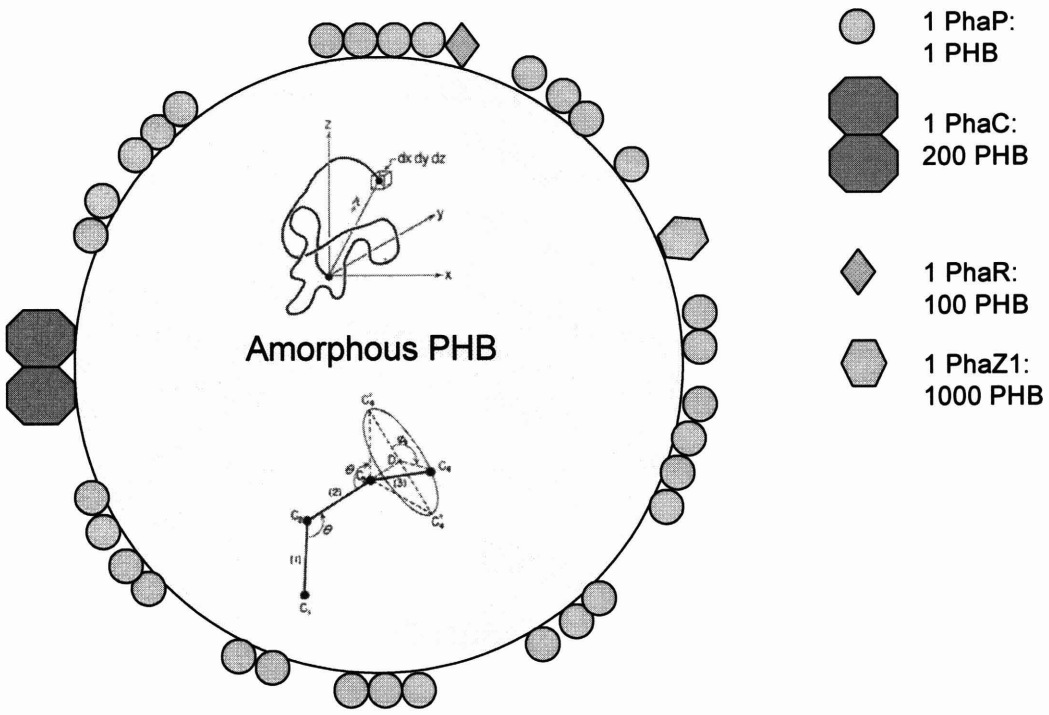

Figure 41. Schematic of the Stabilization Layer on Native PHB Inclusions.

CHAPTER 4.CONCLUSIONS

1. PHB inclusions in a native state without with proteins (PhaP and PhaC) intact at the surface were isolated from *C. necator*. The purified inclusions subjected to elemental analysis, SDS-PAGE, western blots, ^{13}C NMR, and microscopy.

2. Granule diameter was obtained by AFM measurements. The granules, oval or round in shape, have an average diameter of approximately 550nm +/- 100nm. TEM indicates diameters between 200 – 500nm (55).

3. ^{13}C NMR spectra confirmed that the PHB exists in an amorphous state with a density between 1.19 – 1.22 g/cm^3 as indicated by density gradient ultracentrifugation. The PHB molecular chain was modeled considering a random chain conformation a chain overwrap number of 1.8 described the amorphous state of native inclusion PHB.

4. PHB related proteins exist on the isolated PHB inclusions surface as confirmed SDS-PAGE, western blot , and AFM. The average diameter of the globules observed on the inclusion surface was measured as 3.1nm +/- 0.4nm which is within the range of estimated inclusion associated proteins (2.1nm – 3.5nm). The surface charge on the PHB inclusions as determined by zeta potential measurements is $1e/70nm^2$.

5. The model of PHB inclusion proposed integrates experimental data from this study and published work to represent our current understanding of the structure of native PHB granules. This model combines amorphous PHB overwrap number and density, surface charge density, surface protein coating, and size of inclusions and globule proteins based on AFM analysis. This model, it is hoped, will serve as a drawing board for overall understanding the structural property-function relationship of PHB inclusions and PHB biosynthesis.

CHAPTER 5.RECOMMENDATIONS FOR FUTURE WORK

Preventing granule aggregation, together with maintaining amorphous PHB and granule associated proteins, resulted in a purification technique that produced high resolution AFM images of native PHB granules. This purification technique can be used as a tool to study inclusion morphology. As a first step, identification and confirmation of the objects on the surface of the PHB inclusions could be conducted by immunogold labeling granule associated proteins (PhaP, PhaC, PhaR, PhaZ) and imaging the surface of the granules. This technique has been used in the past with DNA (45), and AFM images can distinguish the location of the gold label. Since the material properties of gold colloids differ from that of globular proteins, potentially the labeled proteins can be differentiated from the unlabelled proteins using AFM. This experiment may allow a direct identification of protein of the granule surface as was envisioned for this study.

Dennis et al. claimed that there are two are smooth and rough inclusions(4). The smooth inclusions may have lost the protein coating, and therefore may be in a crystalline state. The surface and mechanical property differences between smooth and rough inclusions could be explored further with AFM nanoindentation conducted on the surface of the inclusions, and differentiate the surface features of protein covered versus exposed PHB chain inclusions.

Finally, in order to complement the AFM and microscopy studies, further biochemical analysis of purified inclusion composition could be conducted. In particular, very little is understood about the putative monolipid layer of the surface of inclusions. Using inclusions isolated in this study an analysis of lipid content can be conducted. This could determine if lipids are present, and if present the relative amount of lipid to inclusion PHB estimated.

CHAPTER 6.APPENDICES

6.1. PhaP PURIFICATION

PhaP was isolated according to the protocol described in the materials and methods section in order to obtain a standard from which to identify PhaP in isolated inclusions. The results of the purification are shown the gel below.

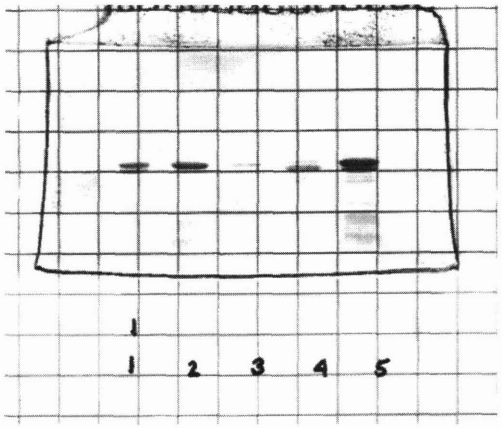

Figure 42. Fractions of Isolated PhaP.

(1) Some intact/some clipped PhaP (2) Almost all intact PhaP (3) Almost all intact PhaP (4) Almost all clipped PhaP (5) Some intact/some clipped PhaP.

6.2 PURIFYING PHB INCLUSIONS ON GLASS USING ANTIBODY

6.2.1. Purification of IgG fraction of Antibody

1ml of Protein A Sepharose FF (GE Healthcare, Piscataway, NJ, Cat# 17-1279-01) was packed into a 0.5cm diameter glass column and the column was equilibrated with 50ml of binding buffer (20mM sodium phosphate pH 7) at 4°C. 1ml of rabbit anti-PhaP blood serum was

loaded onto the column and the flow through was collected. Ten 1ml fractions were collected while flowing binding buffer through the column. The flow rate of buffer through the column was kept at a rate below 1ml/min for the whole experiment. Seven, 1 ml fractions were collected in tubes containing 100µl titration buffer (1M Tris-HCl pH 9) while flowing elution buffer (0.1M sodium citrate pH 3) through the column. The column was washed with 50ml of dH_2O, 5ml of elution buffer, and then 50ml of binding buffer in order to regenerate the column. The A_{280} for each of the column fractions was recorded using a spectrophotometer. Fractions containing a significant amount of protein were collected and run on an SDS PAGE gel (10ug protein/lane). The fractions containing IgG were pooled using amicon ultra filter (Billerica, MA, Cat# UFC901008) by centrifugation at 4°C, 5000 rpm, and 15 min, and stored in buffer containing a final concentration of 0.2% NaN_3 at 4°C.

6.2.2. Acetone Powder Purification

Acetone powders were prepared by growing *ΔphaP* (or *ΔphaC*) cell culture after 75 h on PHB_H media, which was centrifuged down to around 5.75g wet weight of pellet (strains courtesy of the Sinskey Lab, MIT). The pellet was resuspended in 6ml of 0.85% saline and left on ice for 5 minutes. 0.46ml of –20°C acetone was added to the solution which was then vortexed vigorously and then left to incubate at 0°C for 30 min. The resulting precipitate was centrifuged at 12,000 X g for 10 min. The pellet was resuspended in fresh acetone (35ml, -20°C) with vigorous vortex mixing and then allowed to incubate at 0°C for 10 min. Pellet was collected by centrifugation at 12,000 X g for 15 min, and then transferred to filter paper and allowed to air dry at room temperature overnight. The dried pellet was then crushed using mortar and pestle, and then stored in an airtight container at room temperature. The total acetone powder obtained was 456mgs per 5.75 g wet weight of cells.

800µl of anti-PhaP (or anti-PhaC) blood serum was incubated with 100mg of *ΔphaP* (or *ΔphaC*) acetone powder at 4°C with periodic mixing for 30 min. Supernatant from 12 min centrifugation at 12,000 X g was isolated and incubated with another 100mg of *ΔphaP* (or *ΔphaC*) acetone powder at 4°C with periodic mixing for 30 min. The resulting solution was

centrifuged at 12,000 X g for 12 minutes and the resulting supernatant was the acetone powder purified blood serum.

6.2.3. Antibody Attachment to NHS coated glass slides

Purified IgG from anti-PhaP blood serum was incubated on NHS coated class (Nanocs, New York, NY Cat#: NGS 0002) slide for 20 h. The slide was washed with 1% ethanolamine for 30 minutes. The slide was then washed with PBS (pH 7.3-7.5) for 30 min, which was followed by a wash with BlockAid (Invitrogen, Carlsbad, CA, Cat# B-10710) diluted with and equal volume of PBST (PBST = PBS with 0.1% Tween 20). This was followed 2 X 5 min PBST washes. The slide was then washed with secondary antibody (all developing reagents were from Western Light Kit, 2ul in 10ml PBST) for 1 hour, followed by 2 X 5 min PBST washes, 2 X 2 min assay buffer washes, and finally incubation with 3ml of CSPD development solution for 5 min. The slide was developed using chemiluminescence at high sensitivity (10 min development time).

6.2.4. Antigen attachment to Antibody coated glass slides

Purified IgG from anti-PhaP blood serum was incubated on NHS coated glass slide for 20 h. The slide was washed with 1% ethanolamine for 30 min. The slide was then washed with PBS (pH 7.3-9.5) for 30 min, which was followed with BlockAid wash (1 BloackAid: 1 PBST, PBST = PBS with 0.1% Tween 20). The slide was then washed with DH5ά/pGY3a+ cell lysate (strain courtesy of the Sinskey Lab, MIT) for 2 h, followed by 2 X 5 min PBST washes. The culturing procedure for DH5ά/pGY3a+ is explained at the end of the protocol. This was followed with an Anti-GFP (Abcam, Cambridge, MA, Cat# ab6661-100) wash for 1 h (3µl in 10ml), 3 X 5 minute PBST washes, 2 X 2 min assay buffer washes, and finally a 3ml CSPD substrate incubation for 5 min. The slide was placed in development folder and developed for 10 min using chemiluminescence at high sensitivity.

6.2.5. DH5ά/pGY3a+ culture and lysis conditions

40ml of 24 h 100ml LB media culture was centrifuged and resuspended in 10ml of PBS. 1ml of *E.coli* protease inhibitor cocktail was added. 10ml of cell suspension was sonicated for 4 min on high (30 sec pulse, 15 sec pause). 1ml of protease inhibitor cocktail was added cell lysate. DH5ά/pGY3a+ is a strain of *E. coli* that constitutively expresses PhaP-GFP.

6.2.6. Specific Interaction between Antibody and PHB Inclusions

Four 26µl 0.5 mg/ml spots of antibody (IgG fraction, rabbit polyclonal) were placed on an NHS coated glass slide and allowed to incubate for overnight and 30 min at RT and PH:7.3-7.5. The four spots were the following:

i. 1 = IgG purified from anti-PhaP blood serum
ii. 2 = IgG purified from anti-PhaC blood serum
iii. 3 = anti-GFP (Invitrogen, Carlsbad, CA, Cat# A11122)
iv. 4 = anti-MYC (Upstate, Charlottesville, VA, Cat# 06-549)

The slide was washed with 1% ethanolamine for 1 h, followed by a wash with BlockAid (1:1 PBST) for 1 h, and then a PBST wash for 5 min. The slide was then washed with RE1018 (strain courtesy of the Sinskey Lab, MIT) cell lysate for 30 min. The RE1018 culture condition are detailed at the end of this protocol, this was followed with 3 X 5 min PBS washes. The slide was then washed with anti-GFP (all developing reagents were from Western Light Kit, 3µl in 10ml PBS) for 1 h, followed by 3 X 5 min PHS washes, 2 X 2 minute assay buffer washes, and finally 3ml CSPD incubation for 5 min. The slide was placed in a plastic development folder and imaged using chemiluminescence superhigh sensitivity for 10 min exposure.

6.2.7. RE1018 culture and lysis conditions

A 48 h PHBH culture (50ml) was centrifuged down and resuspended in 1 ml protease inhibitor cocktail, 1 ml PBS, and 50mg lysozyme and left to incubate at 37°C for 1 h. 0.5ml of

5M NaCl was added along with 20µl of DNase (10U/µl) and the solution was incubated at 37°C for 1 h. The cell lysate was brought up to a final volume of 10ml with PBS. RE1018 is a *C. necator* strain that expresses PhaP-GFP, rather than wildtype phasin.

6.2.8. Methodology

6.2.8.1. Anti-PhaP IgG

Anti-PhaP IgG fraction was purified in order to have a relatively pure and sufficient amount of anti-PhaP with which to work with for the surface chemistry experiments. The results are shown in the gel below.

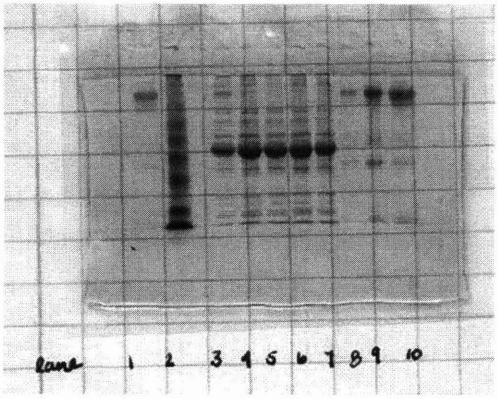

Figure 43. Isolated Fractions of Anti-PhaP IgG.
(1), (8), (9), (10) flow through fractions (2) MW standard (3), (4), (5), (6), (7) Anti-PhaP IgG fractions

6.1.8.2 Anti-PhaC IgG

Anti-PhaC IgG fraction was purified in order to have a relatively pure and sufficient amount of anti-PhaC with which to work with for the surface chemistry experiments. The results are shown in the gel below

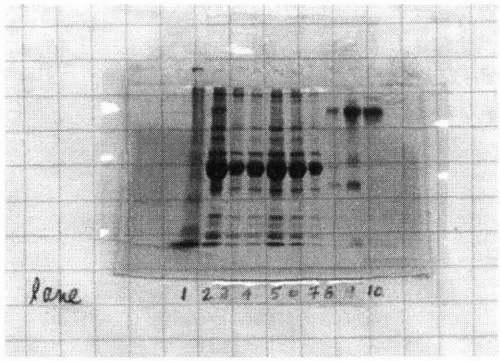

Figure 44. Isolated Fractions of Anti-PhaC IgG.
(1) MW standard (2) – (7) Anti-PhaC IgG fractions, (8) – (10) flow through fractions

6.2.8.3. Acetone Powder Effectiveness

Acetone powders were made and incubated with anti-PhaP in order to determine whether they were able to purify the PhaP one step further. Based on the results of western blots that used acetone treated anti-PhaP and regular acetone powder, it was determined that acetone powders were not increasing the purity of the antibody, but rather served to decrease the activity of the antibody.

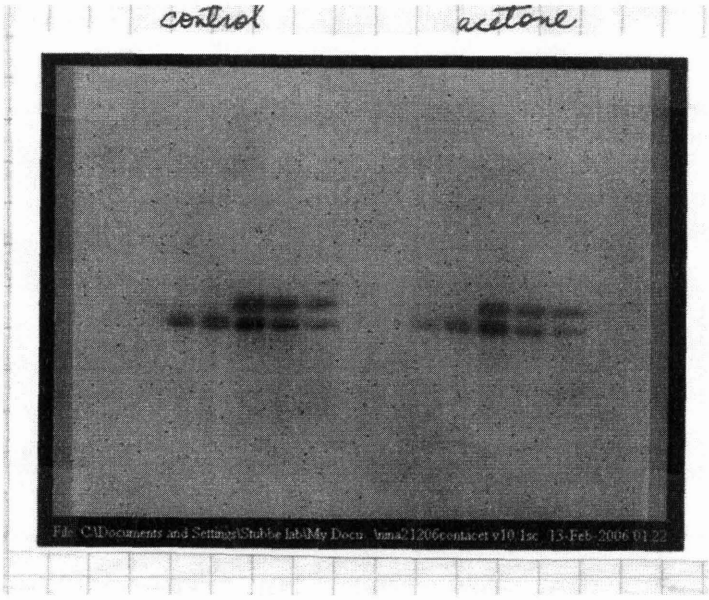

Figure 45. Regular anti-PhaP to detect PhaP (right) & Acetone powder treated anti-PhaP to detect PhaP (left)

6.2.8.4. Monitoring Attachment onto Glass Slide

An attempt to develop an affinity slide that selects PHB from a solution of cell lysate, by use of antibodies was attempted. The results of the preliminary experiments are shown in the figure below.

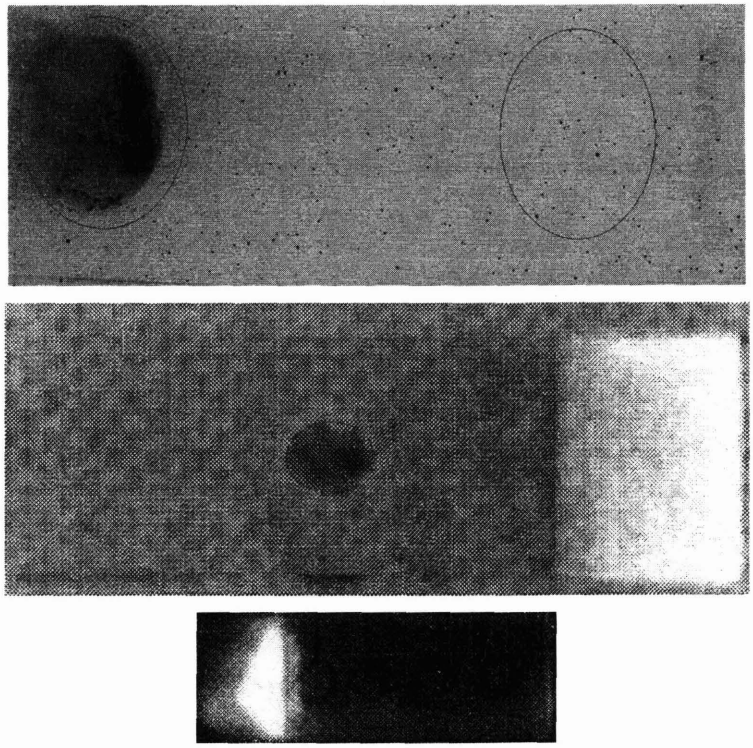

Figure 46. Monitoring Attachment to Glass Slide with Chemiluminescence.
(Top) Covalent attachment of anti-PhaP IgG to NHS coated glass slide as indicated by chemiluminescence. (Middle) Binding of PhaP-GFP onto anti-PhaP IgG/NHS coated glass slide as indicated by chemiluminescence. (Bottom) Non-specific binding of PHB (PhaP-GFP strain) with antibody treated spots on NHS coated glass slide. Four spots from left to right anti-PhaP IgG, anti-PhaC IgG, anti-GFP IgG, anti-myc IgG (negative control).

CHAPTER 7. REFERENCES

1. Anderson, A. J., and E. A. Dawes. 1990. Occurrence, metabolism, metabolic role, and industrial uses of bacterial polyhydroxyalkanoates. Microbiol Rev 54: 450-472.

2. Barnard, G. N., and J. K. M. Sanders. 1989. The poly-beta-hydroxybutyrate granule *in vivo* . A new insight based on NMR spectroscopy of whole cells. J. Biol. Chem. 264: 3286-3291.

3. Boatman, E. S. 1964. Observation of the fine structure of spheroplasts of *Rhodospirillum rubrum* . J Cell Biol 20: 297-311.

4. Dennis, D., C. Liebig, T. Holley, K. S. Thomas, A. Khosla, D. Wilson, and B. Augustine. 2003. Preliminary analysis of polyhydroxyalkanoate inclusions using atomic force microscopy. FEMS Microbiology Letters 226: 113-119.

5. Ellar, D., D. G. Lundgren, K. Okamura, and R. H. Marchessault. 1968. Morphology of poly-beta-hydroxybutyrate granules. J. Mol. Biol. 35: 489-502.

6. Flory, P. 1953. Principles of Polymer Chemistry. Cornell University Press, Ithaca.

7. Fuller, R. C. 1999. Microbial inclusions with special reference to PHA inclusions and intracellular boundary envelopes. Int J Biol Macromol 25: 21-9.

8. Gerngross, T. U., P. Reilly, J. Stubbe, A. J. Sinskey, and O. P. Peoples. 1993. Immunocytochemical analysis of poly-beta-hydroxybutyrate (PHB) synthase in *Alcaligenes eutrophus* H16: localization of the synthase enzyme at the surface of PHB granules. J Bacteriol 175: 5289-5293.

9. Gerngross, T. U., K. D. Snell, O. P. Peoples, A. J. Sinskey, E. Csuhai, S. Masamune, and J. Stubbe. 1994. Overexpression and purification of the soluble polyhydroxyalkanoate synthase from *Alcaligenes eutrophus* : evidence for a required posttranslational modification for catalytic activity. Biochemistry 33: 9311-9320.

10. Griebel, R. J., and J. M. Merrick. 1971. Metabolism of poly- -hydroxybutyrate: effect of mild alkaline extraction on native poly-β-hydroxybutyrate granules. J Bacteriol 108: 782-9.

11. Hanley, S. Z., D. J. Pappin, D. Rahman, A. J. White, K. M. Elborough, and A. R. Slabas. 1999. Re-evaluation of the primary structure of *Ralstonia eutropha* phasin and implications for polyhydroxyalkanoic acid granule binding. FEBS Lett. 447: 99-105.

12. Haywood, G. W., A. J. Anderson, and E. A. Dawes. 1989. The Importance of PHB-Synthase Substrate-Specificity in Polyhydroxyalkanoate Synthesis by Alcaligenes-Eutrophus. Fems Microbiology Letters 57: 1-6.

13. Hobbs, J. K., T. J. McMaster, M. J. Miles, and P. J. Barham. 1998. Direct observations of the growth of spherulites of poly(hydroxybutyrate-co-valerate) using atomic force microscopy. Polymer 93: 2437-2446.

14. Horowitz, D. M., and J. K. M. Sanders. 1994. Amorphous, Biomimetic Granules of Polyhydroxybutyrate - Preparation, Characterization, and Biological Implications. Journal of the American Chemical Society 116: 2695-2702.

15. Israelachvili, J. 1991. Intermolecular & Surface Forces, 2 ed. Academic Press, London.

16. Jendrossek, D., and R. Handrick. 2002. Microbial degradation of polyhydroxyalkanoates. Annu Rev Microbiol 56: 403-32.

17. Jendrossek, D., A. Schirmer, and H. G. Schlegel. 1996. Biodegradation of polyhydroxyalkanoic acids. Appl. Microbiol. Biotechnol. 46: 451-463.

18. Jossek, R., R. Reichelt, and A. Steinbüchel. 1998. *In vitro* biosynthesis of poly(3-hydroxybutyric acid) by using purified poly(hydroxyalkanoic acid) synthase of *Chromatium vinosum*. Appl Microbiol Biotechnol 49: 258-266.

19. Jurasek, L., and R. H. Marchessault. 2002. The role of phasins in the morphogenesis of poly(3-hydroxybutyrate) granules. Biomacromolecules 3: 256-61.

20. Kawaguchi, Y., and Y. Doi. 1990. Structure of Native Poly(3-Hydroxybutyrate) Granules Characterized by X-Ray-Diffraction. Fems Microbiology Letters 70: 151-156.

21. Kobayashi, T., M. Shiraki, T. Abe, A. Sugiyama, and T. Saito. 2003. Purification and properties of an intracellular 3-hydroxybutyrate-oligomer hydrolase (PhaZ2) in *Ralstonia eutropha* H16 and its identification as a novel intracellular poly(3-hydroxybutyrate) depolymerase. J Bacteriol 185: 3485-90.

22. Kobayashi, T., K. Uchino, T. Abe, Y. Yamazaki, and T. Saito. 2005. Novel intracellular 3-hydroxybutyrate-oligomer hydrolase in *Wautersia eutropha* H16. J Bacteriol 187: 5129-35.

23. Komoroski, R. A. 1986. HIgh Resolution NMR Spectroscopy of Synthetic Polymers in Bulk. VCH Publishers, Inc, New York.

24. Lemoigne, M. 1926. Produits de deshydration et de polymerisation de l'acide β -oxybutyric. Bull. Soc. Chim. Biol. (Paris) 8: 770-782.

25. Lenz, R. W., and R. H. Marchessault. 2005. Bacterial polyesters: biosynthesis, biodegradable plastics and biotechnology. Biomacromolecules 6: 1-8.

26. Liebergesell, M., K. Sonomoto, M. Madkour, F. Mayer, and A. Steinbuchel. 1994. Purification and characterization of the poly(hydroxyalkanoic acid) synthase from *Chromatium vinosum* and localization of the enzyme at the surface of poly(hydroxyalkanoic acid) granules. Eur J Biochem 226: 71-80.

27. Lundgren, D. G., R. Alper, C. Schnaitman, and D. H. Marchessault. 1965. Characterization of Poly- β -Hydroxybutyrate Extracted from Different Bacteria. J Bacteriol 89: 245-251.

28. Lutke-Eversloh, T., J. Kawada, R. H. Marchessault, and A. Steinbuchel. 2002. Characterization of microbial polythioesters: physical properties of novel copolymers synthesized by *Ralstonia eutropha*. Biomacromolecules 3: 159-66.

29. Madison, L. L., and G. W. Huisman. 1999. Metabolic engineering of poly(3-hydroxyalkanoates): from DNA to plastic. Microbiol. Mol. Biol. Rev. 63: 21-53.

30. Marchessault, R. H., K. Okamura, and C. J. Su. 1970. Physical properties of poly(β -hydroxybutyrate). II. Conformational aspects in solution. Macromolecules 3: 735-740.

31. Merrick, J. M., and M. Doudoroff. 1964 Depolymerization of Poly- β -Hydroxybutyrate by an Intracellular Enzyme System. J Bacteriol 88: 60-71.

32. Merrick, J. M., D. G. Lundgren, and R. M. Pfister. 1965. Morphological Changes in Poly-Beta-Hydroxybutyrate Granules Associated with Decreased Susceptibility to Enzymatic Hydrolysis. J Bacteriol 89: 234-9.

33. Merrick, J. M., R. Steger, and D. Dombroski. 1999. Hydrolysis of native poly(hydroxybutyrate) granules (PHB), cystalline PHB, and artificial amorphous PHB granules by intracellular and extracellular depolymerases. Int J Biol Macromol 25: 129 - 134.

34. Okamura, K., and R. H. Marchessault. 1967. Presented at the International Symposium on the Conformation of Biopolymers, University of Madras, India.

35. Peoples, O. P., and A. J. Sinskey. 1989. Poly-beta-hydroxybutyrate (PHB) biosynthesis in *Alcaligenes eutrophus* H16. Identification and characterization of the PHB polymerase gene (*phbC*). J. Biol. Chem. 264: 15298-15303.

36. Peoples, O. P., and A. J. Sinskey. 1989. Poly-beta-hydroxybutyrate biosynthesis in *Alcaligenes eutrophus* H16. Characterization of the genes encoding beta-ketothiolase and acetoacetyl-CoA reductase. J. Biol. Chem. 264: 15293-15297.

37. Potter, M., H. Muller, F. Reinecke, R. Wieczorek, F. Fricke, B. Bowien, B. Friedrich, and A. Steinbuchel. 2004. The complex structure of polyhydroxybutyrate (PHB) granules: four orthologous and paralogous phasins occur in *Ralstonia eutropha* . Microbiology 150: 2301-11.

38. Potter, M., and A. Steinbuchel. 2005. Poly(3-hydroxybutyrate) granule-associated proteins: impacts on poly(3-hydroxybutyrate) synthesis and degradation. Biomacromolecules 6: 552-60.

39. Rehm, B. H. 2003. Polyester synthases: natural catalysts for plastics. Biochem J 376: 15-33.

40. Saegusa, H., M. Shiraki, C. Kanai, and T. Saito. 2001. Cloning of an intracellular Poly[D(-)-3-Hydroxybutyrate] depolymerase gene from *Ralstonia eutropha* H16 and characterization of the gene product. J Bacteriol 183: 94-100.

41. Sanders, J. K., and B. K. Hunter. 1993. Modern NMR Spectroscopy: A Guide for Chemists, 2nd ed. Oxford University Press, Inc, New York.

42. Schwartz, E., A. Henne, R. Cramm, T. Eitinger, B. Friedrich, and G. Gottschalk. 2003. Complete nucleotide sequence of pHG1: a *Ralstonia eutropha* H16 megaplasmid encoding key enzymes of H(2)-based ithoautotrophy and anaerobiosis. J Mol Biol 332: 369-83.

43. Seo, M. C., H. D. Shin, and Y. H. Lee. 2003. Functional role of granule-associated genes, *phaP* and *phaR*, in poly-beta-hydroxybutyrate biosynthesis in recombinant *E-coli* harboring *phbCAB* operon. Biotechnology Letters 25: 1243-1249.

44. Seo, M. C., H. D. Shin, and Y. H. Lee. 2004. Transcription level of granule-associated *phaP* and *phaR* genes and granular morphogenesis of poly-beta-hydroxyalkanoate granules in *Ralstonia eutropha.* Biotechnology Letters 26: 617-622.

45. Shaiu, W. L., D. D. Larson, J. Vesenka, and E. Henderson. 1993. Atomic force microscopy of oriented linear DNA molecules labeled with 5nm gold spheres. Nucleic Acids Res 21: 99-103.

46. Shaw, G. L., M. K. Melby, D. M. Horowitz, J. Keeler, and J. K. Sanders. 1994. Nuclear magnetic resonance relaxation studies of poly(hydroxybutyrate) in whole cells and in artificial granules. Int J Biol Macromol 16: 59-63.

47. Slater, S. C., W. H. Voige, and D. E. Dennis. 1988. Cloning and expression in *Escherichia coli* of the *Alcaligenes eutrophus* H16 poly-beta-hydroxybutyrate biosynthetic pathway. J Bacteriol 170: 4431-6.

48. Steinbüchel, A., and H. E. Valentin. 1995. Diversity of bacterial polyhydroxyalkanoic acids. FEMS Microbiol. Lett. 128: 219-228.

49. Stubbe, J., A. He, J. Tian, A. G. Lawrence, P. Liu, and A. J. Sinskey. 2005. Expression and Analysis of Proteins Involved in Polyhydroxybutyrate Homeostasis in *Wautersia eutropha* H16.

50. Stubbe, J., J. Tian, A. He, A. J. Sinskey, A. G. Lawrence, and P. Liu. 2005. Nontemplate-dependent polymerization processes: polyhydroxyalkanoate synthases as a paradigm. Annu Rev Biochem 74: 433-80.

51. Sudesh, K., H. Abe, and Y. Doi. 2000. Synthesis, structure and properties of polyhydroxyalkanoates: biological polyesters. Prog. Polym. Sci. 25: 1503-55.

52. Sudesh, K., A. Maehara, Z. Gan, I. Tadahisa, and Y. Doi. 2004. Direct observation of polyhydroxyalkanoate granule-associated-proteins on native granules and on poly(3-hydroxybutyrate) single crystals by atomic force microscopy. Polymer Degradation and Stability 83: 281-287.

53. Tian, J., A. He, A. G. Lawrence, P. Liu, N. Watson, A. J. Sinskey, and J. Stubbe. 2005. Analysis of transient polyhydroxybutyrate production in *Wautersia eutropha* H16 by quantitative Western analysis and transmission electron microscopy. J Bacteriol 187: 3825-32.

54. Tian, J., A. J. Sinskey, and J. Stubbe. 2005. Class III polyhydroxybutyrate synthase: involvement in chain termination and reinitiation. Biochemistry 44: 8369-77.

55. Tian, J., A. J. Sinskey, and J. Stubbe. 2005. Kinetic studies of polyhydroxybutyrate granule formation in *Wautersia eutropha* H16 by transmission electron microscopy. J Bacteriol 187: 3814-24.

56. Townsend, K. J., K. Busse, J. Kressler, and C. Scholz. 2005. Contact angle, WAXS, and SAXS analysis of poly(beta-hydroxybutyrate) and poly(ethylene glycol) block copolymers obtained via *Azotobacter vinelandii* UWD. Biotechnol Prog 21: 959-64.

57. Vesenka, J., S. Manne, R. Giberson, T. Marsh, and E. Henderson. 1993. Colloidal gold particles as an incompressible atomic force microscope imaging standard for assessing the compressibility of biomolecules. Biophys J 65: 992-7.

58. Wieczorek, R., A. Pries, A. Steinbuchel, and F. Mayer. 1995. Analysis of a 24-kilodalton protein associated with the polyhydroxyalkanoic acid granules in *Alcaligenes eutrophus* . J Bacteriol 177: 2425-35.

59. Wieczorek, R., A. Steinbüchel, and B. Schmidt. 1996. Occurrence of polyhydroxyalkanoic acid granule-associated proteins related to the *Alcaligenes eutrophus* H16 GA24 protein in other bacteria. FEMS Microbiol Lett 135: 23-30.

60. Wind, M., R. Graf, S. Renker, H. W. Spiess, and W. Steffen. 2005. Structure of amorphous poly-(ethylmethacrylate): a wide-angle x-ray scattering study. J Chem Phys 122: 14906.

61. York, G. M. 2002. York-USB-04-17-02.ppt. Massachusetts Institute of Technology.

62. York, G. M., J. Lupberger, J. Tian, A. G. Lawrence, J. Stubbe, and A. J. Sinskey. 2003. *Ralstonia eutropha* H16 encodes two and possibly three intracellular Poly[D-(-)-3-hydroxybutyrate] depolymerase genes. J Bacteriol 185: 3788-94.

63. York, G. M., J. Stubbe, and A. J. Sinskey. 2001. New insight into the role of the PhaP phasin of *Ralstonia eutropha* in promoting the synthesis of polyhydroxybutyrate. J. Bacteriol. 183: 2394-2397.

64. York, G. M., J. Stubbe, and A. J. Sinskey. 2002. The *Ralstonia eutropha* PhaR protein couples synthesis of the PhaP phasin to the presence of polyhydroxybutyrate in cells and promotes polyhydroxybutyrate production. J Bacteriol 184: 59-66.

65. Zhang, S. M., S. Kolvek, R. W. Lenz, and S. Goodwin. 2003. Mechanism of the polymerization reaction initiated and catalyzed by the polyhydroxybutyrate synthase of *Ralstonia eutropha*. Biomacromolecules 4: 504-509.